UNIVERSITY OF CALIFORNIA, DAVIS

BERKELEY • DAVIS • IRVINE • LOS ANGELES • RIVERSIDE • SAN DIEGO • SAN FRANCISCO

SANTA BARBARA • SANTA CRUZ

DEPT. OF LAND, AIR AND WATER RESOURCES
151 HOAGLAND HALL
(530) 752-1406
FAX (530) 752-1552
HTTP://LAWR.UCDAVIS.EDU

ONE SHIELDS AVENUE
DAVIS, CALIFORNIA 95616-8627

February 24, 2016

Dear editor,

The responses to two reviewers' comments and the tracking version of the revised manuscript are attached to this letter. Thank you very much for your time and help

Regards,

Shu-Hua Chen
Professor
E-mail: shachen@ucdavis.edu
Tel: 530-752-1822

Anonymous Referee #1

As some reviewers pointed out in previous submission, the simulation improvement of the new source-oriented approach is marginal but the computational cost increases a lot. The application of such method in operational forecasts is deemed to be impractical. Therefore, the current study raises speculations from readers about the importance of the new methodology. The best way to demonstrate the merit of the approach is to conduct idealized simulations under highly controlled conditions to explore the sensitivity of simulated clouds and radiative feedback to a wide range of parameter space. Then the best application of this methodology is to come up with novel parameterizations based on idealized results that can improve the simulations by the simple approach, such as the internal mixture method.

Reply: The authors appreciate the reviewer's suggestions on a different research aspect of using a source-oriented atmosphere-chemistry model. We would like to point out that both types of studies are important as each has its own merit and both should be encouraged. The first type of studies, suggested by the reviewer, is to improve the parameterizations of cloud activation, ice nucleation and aerosol internal mixing in numerical models. This type of study is important and can be very beneficial to the scientific community and most importantly to the operational centers. However, since cloud and aerosol microphysical processes can vary significantly in time and space and are highly nonlinear, it is difficult to parameterize for a wide range of weather and air pollution conditions, in particular for extreme ones. Thus directly applying source-oriented (i.e., aerosol external mixture) models to study real cases, the second type of studies, should be considered if computational resources are affordable. The source-oriented approach is an original approach, which has fewer assumptions and thus can be applied to a wider range of conditions. The purpose of the study is not to improve the internal mixture parametrization, but to assess the influence of different aerosol mixture methods on fog formation, cloud optical properties and the surface energy budget using exactly the same model, except the aerosol mixture methods.

In scientific communities, using simplified parametrization in numerical simulations is often under the constraint of computational power and/or the limitation of numerical tools. Since we have both, it seems a natural step to move onto the next stage of research, directly applying a source-oriented model to study aerosol-cloud-radiation interactions.

In the past decades numerical studies on Tule fog have been rare. This is in part due to model's difficulty to simulate fog reasonably. We chose this challenging weather system for our first study of this kind since Tule fog is important in safety, hydrology and agriculture in California. But more importantly fog is an excellent scientific subject that can isolate cloud activation and diffusive growth, the first step of aerosol-cloud-radiation interactions, from other microphysical processes which usually do not occur in fog. Compared to the internal mixture method, the source-oriented method does improve model results (even if the effect in this case is slight) which is in fact a positive contribution to the science. The modest amount of improvement implies that the parameterization of the internal mixture method provides a good approximation to the external mixture method for the studies of fog, a mild weather phenomenon. However, this does not imply that the internal mixture method will do well for other

weather and pollution conditions, in particular for those very nonlinear weather systems. The reason why we chose this particular phenomenon for our first study has mentioned above. We are now conducting more numerical studies on different weather systems to explore the full range of responses. We have added the following in the revised manuscript.

"We chose this challenging weather system for the first study of this kind since Tule fog is important in safety, hydrology and agriculture in California. Fog is also an excellent scientific case study that can isolate cloud activation and diffusive growth, the first step of aerosol-cloud-radiation interactions, from other microphysical processes which usually do not occur in fog." Line 274-278.

"**We are now conducting more numerical studies on different weather systems to explore the full range of responses."** Lines 632-633.

Anonymous Referee #2

This paper well describes the impacts of source-oriented aerosols and aerosol-cloud interaction on fog formation by implementing the modified cloud microphysics and radiation schemes into the source-oriented Weather Research and Forecasting chemistry model (SOWC). Here are some major and specific comments, which need to be considered before the publication.

The authors appreciate the reviwer's comments. Follows are point-by-point response to the reviewer's comments. *The bolded texts are added in the revised manuscript according to reviewer's comments.*

1. The authors noted in section3 that the computational cost of the SOWC model simulation is 25 times higher than that of the standard WRF/Chem simulation. Known that the SOWC model is computationally very expensive, how can authors conclude that the SOWC model should be a useful public model to predict effects of climate change on the hydrological cycle and energy budget?

Reply: The standard WRF/Chem simulation we mentioned in the manuscript is the WRF/Chem model with prescribed aerosols (chem_opt = 0), which does not include any chemistry processes. In general, the computational cost of WRF/Chem with any chemistry option (/=0) is about 5 times of that with chem_opt = 0 in the released WRF/Chem 3.1.1 version. Thus, the computational time of SOWC is about 5 times of WRF/Chem with any chemistry option (/=0). Although the SOWC model still has a higher computational demand and is probably not feasible for all users, it should be a useful tool to users who are able to access super computers or computer clusters to conduct research relevant to aerosol-cloud-radiation interactions. With rapidly growing CPU efficiency and computing resources it seems a natural step to move on to the next stage of research for pursuing a more comprehensive method with fewer assumptions, like the source-oriented method, to study aerosol-cloud-radiation interactions.

We appreciate the reviewer's comment and have modified "the SOWC model should be a useful public model to study aerosol-cloud-radiation interactions and to predict the effects of climate change on the hydrological cycle and energy budget." to **"the SOWC model should be a useful tool to study aerosol-cloud-radiation interactions"** in Lines 631-632. We have also modified the manuscript to **"The computational cost of the SOWC model, which is proportional to the extra information that is tracked, is approximately 25 times greater than the standard WRF/Chem 3.1.1 simulation with prescribed aerosols (chem_opt = 0) or approximately 5 times greater than the standard WF/Chem 3.1.1 simulation with any chemistry option (/=0) in the current study."** Please also see Lines 370-374.

2. Substantial efforts, modification of radiation schemes to interact with cloud droplets (section 2-3), has been put in this paper to study aerosol-cloud interactions during fog simulations. Why did the authors select the fog event that occurred under calm and stable meteorological condition, which is responsible for similar model results between 'S_ARon_CRmod' and 'S_ARon_CRorig' (see last paragraph in section 4-2)? How will simulation results be affected by the modified calculation method of cloud optical property if we choose different fog cases?

Reply: We have described why a fog case was chosen in response to the other reviewer's comments. In the past decades numerical studies on Tule fog have been rare. This is in part due to model's difficulty to simulate fog reasonably. "**We chose this challenging weather system for our first study of this kind since Tule fog is important in safety, hydrology and agriculture in California. Fog is an excellent scientific case study that can isolate cloud activation and diffusive growth, the first step of aerosol-cloud-radiation interactions, from other microphysical processes which usually do not occur in fog."** The fog case that we chose is a very typical case and thus should be quite representative for a Tule fog event. Thus, for other fog cases the results might be different because the model can perform differently, better or worse, but we expect that the conclusion will be similar, if fog is successfully simulated, as the microphysical processes that are involved in fog events are minimal, i.e., only activation and diffusion growth. We are conducting more numerical studies for different type of weather systems using the SOWC model. In this revised version, we have added additional explanation why we chose a fog event for the study. The above bolded text is added in the revised manuscript at Lines 274-278 to explain why the fog phenomena was chosen for our study.

Note: Another unique feature of the modified radiation scheme in our model is that we also consider aerosol radiative properties in the cloud droplets. Most radiation schemes treat cloud droplets are pure water so cloud optical properties only depend on cloud droplet size (radius). However, in our model the optical properties of soot-activated cloud droplets differ from those of sulfate-activated cloud droplets even if they have the same size. Hence, the simulation results can differ not only because of different fog cases but also because of different CCN chemical components, e.g., when one compares a recent fog event with one twenty years ago.

3. Cloud-droplet number concentration between 'S_ARon_CRmod' and 'S_ARon_CRorig' shows significant differences (the difference is greater than the one between 'S_ARon_CRmod' and 'S_AROff_CRmod'), even though other fields such as Qc, SKT, NSF, LH, and SH are similar between two simulations. Please check the sentences in section 4.2.

Reply: It is true that the difference of the number concentration between 'S_ARon_CRmod' and 'S_ARon_CRorig' is greater than that between 'S_ARon_CRmod' and 'S_AROff_CRmod'. However, the difference of the cloud mixing ratio amount between the former two experiments (0.001 g m^{-3}) is smaller than that between the latter two experiments (0.007 g m^{-3}). This result stems from the fact that more small cloud droplets were evaporated in S_ARon_CRmod after the use of the new cloud-radiation interaction. We have examined the number concentration of each cloud droplet size between 'S_ARon_CRmod' and 'S_ARon_CRorig' to confirm this finding. Please keep in mind that the difference between 'S_ARon_CRmod' and 'S_ARon_CRorig' is *the calculation of the cloud-radiation interaction* with the same microphysics parameterization, while the difference between 'S_ARon_CRmod' and 'S_AROff_CRmod' is due to *the neglect of the aerosol-radiation interaction*. The differences of the cloud optical thickness and net downward shortwave radiation between 'S_ARon_CRmod' and 'S_ARon_CRorig' (0.41 for COT and 0.46 for NSF) are also smaller than those between 'S_ARon_CRmod' and 'S_AROff_CRmod' (1.07 for COT and 3.68 for NSF). Thus,

the differences of the meteorological variables (*SKT, NSF, LH, and SH*) between 'S_ARon_CRmod' and 'S_ARon_CRorig' are small.

In the original radiation scheme S_ARon_CRorig, the cloud droplets are assumed to have uniform size; however, in the modified radiation scheme S_ARon_CRmod, cloud droplet size varies for each bin and source types. Additionally, the formula of cloud optical thickness (COT), single scattering albedo and asymmetry factor in the modified radiation scheme are all updated in S_ARon_CRmod. Cloud optical thickness in the original radiation scheme, for example, is a function of cloud water path (CWP) and effective radius (4 μm ≤ r_e ≤ 20 μm) derived from the total droplet number:

$$\tau_{orig}(\lambda) = CWP \times (-6.59 \times 10^{-3} + \frac{1.65}{r_e}). \quad \text{(s1)}$$

However, in the modified radiation scheme cloud optical thickness is a function of cloud droplet size, number, and chemical composition of each bin / source (Eq. 3 in the manuscript). With a similar Q_c, although Q_n in S_ARon_CRorig is higher than that in S_ARon_CRmod, the COT is slightly higher in S_ARon_CRmod due to different formulas used in the calculation of cloud-radiation interaction. The small difference of COT between these two experiments in fact indicates that the parameterization of COT in the original radiation scheme provides a reasonable result compared to the explicit COT calculation.

We would like to emphasize that our main focus of the manuscript is the difference of the aerosol activation between different mixing states (internal vs. source-oriented mixing) and its impact on a fog event, not the modification of cloud-radiation interaction. However, since the size and number concentration of cloud droplets are available from the SOWC model, we elected to use the information to calculate cloud-radiation optical properties even though this level of detail was not readily available when the radiation scheme was first developed.

We agree that the last sentence in section 4.2 could confuse the readers by assuming the difference between S_ARon_CRmod and S_ARon_CRorig only comes from the size distribution. We have modified it to read **"Although S_ARon_CRorig had slightly higher cloud droplet number concentrations, the modified calculation of the cloud optical properties in S_ARon_CRmod gave a similar cloud amount and net shortwave radiation flux reaching the surface, which produced nearly identical feedbacks to meteorology in both experiments (Table 5)."** Please see Lines 487-490. We also add COT in Table 5 in the revised version.

	S_ARon_CRmod	S_ARon_CRorig	S_AROff_CRmod	I_ARon_CRmod
Q_c^* (g m^{-3})	0.220	0.221	0.213	0.231
Q_n^* (# m^{-3})	3.94×10^8	4.18×10^8	3.77×10^8	4.57×10^8
SKT (K)	281.305	281.30	281.404	281.151
NSF** (W m^{-2})	130.56	131.02	134.24	124.54
LH (W m^{-2})	9.01	9.02	9.36	8.40
SH (W m^{-2})	4.91	4.55	5.27	4.54
COT (unitless)	**25.56**	**25.15**	**24.49**	**28.62**

4. Figure 6 shows that Nitrate concentration in the model is much lower than the observation at all CAAQD stations used in the analysis. How can high Nitrate concentrates in the SJV? What causes high Nitrate concentration in the SJV?

Reply: Nitrate production in the SJV during the winter season primarily occurs via the "dark" chemistry pathway. Background ozone advected into the region from outside California mixes with local NO emissions to form NO_2, NO_3, N_2O_5, and HNO_3 which partitions to condensed particulate nitrate because of cold temperature in the winter. Ying et al. (2009) used a source-oriented air quality model to study source contributions to secondary pollutants formation within California's Central Valley during a severe winter stagnation event during December 2000 – January 2001. In their study, they identified diesel engines as the largest contributor to particle nitrate. Zhang et al. (2014) used the SOWC model to simulate the same episode and studied the effects of particle mixing and feedbacks to meteorology and chemistry without consideration of fogs. More recent simulations for episodes in the year 2010 and later have been unable to reproduce observed nitrate buildup using standalone regional chemical transport models or coupled meteorology-chemical transport models (such as WRF/Chem). The performance of the SOWC model in the current study is typical of such efforts, and considerable new research is directed at improving this feature but results are forthcoming and beyond the scope of the current study.

References:

Ying, Q. and Kleeman, M. J.: Regional contributions to airborne particulate matter in central California during a severe pollution episode, Atmos. Environ., 43, 1218–1228, 2009.

Zhang, H., DeNero, S. P., Joe, D. K., Lee, H.-H., Chen, S.-H., Michalakes, J., and Kleeman, M. J.: Development of a source oriented version of the WRF/Chem model and its application to the California regional PM10 / PM2.5 air quality study, Atmos. Chem. Phys., 14, 485-503, doi:10.5194/acp-14-485-2014, 2014.

5. Please check specific comments shown below.

1) It would be better to show available observations for aerosol concentration to compare with the simulated aerosol concentration. Model produces abundant smaller cloud droplets and high CCN concentration, which causes bias in surface temperature.

Reply: Unfortunately, in this study we only have observations available on 18 January, as shown in Figure 6. "**If more discussion of aerosol perditions from the SOWC model is desired, we refer the reader to Zhang et al. (2014) who present a comparison of predicted aerosol concentrations and measured concentrations using field campaign data measured during the California Regional PM_{10} / $PM_{2.5}$ Air Quality Study (CRPAQS) in December 2000 – January 2001**." (Added in the revised manuscript Line 408-412). To address this question using the indirect measurements available in the current study we have conducted two more experiments. The first new experiment uses WRF default prescribed aerosols (chem_opt = 0). Results show that WRF/Chem still underestimated the surface

temperature. The surface temperature in daytime was even 1~2 °C colder than that in any experiment in this study due to high aerosol concentration (10^9 #/kg-air; Dp = 10 μm). The second new experiment reduces the prescribed aerosol concentration by one order of magnitude. However, simulated fog was not thick enough in the nighttime and the simulated fog completely disappeared late on 16 January under these test conditions.

The results summarized above confirm that radiative fog indeed is a very challenging weather system for numerical simulations and forecasts. In addition to the potential of too many small cloud droplets, there are two more potential reasons that cause the cold bias in the current study. One is the inaccurate aerosol-cloud-radiation interaction, which is a common and challenging problem in numerical models. The other is the complex terrain in Central Valley of California, where thermodynamical and dynamical processes under fog conditions are difficult to simulate (e.g., drainage flow). Improvements in the aerosol-cloud-radiation interaction in complex terrain is very challenging problem facing all coupled atmosphere-chemistry models.

The figures below provide additional comparison between observations and a WRF simulation, which excludes aerosol direct and indirect effects. The WRF model cannot simulate fog without the inclusion of the aerosol effect. The results show a clear diurnal cycle in simulated 2-m temperature (WRF_T2) because the cloud radiative effect is missing.

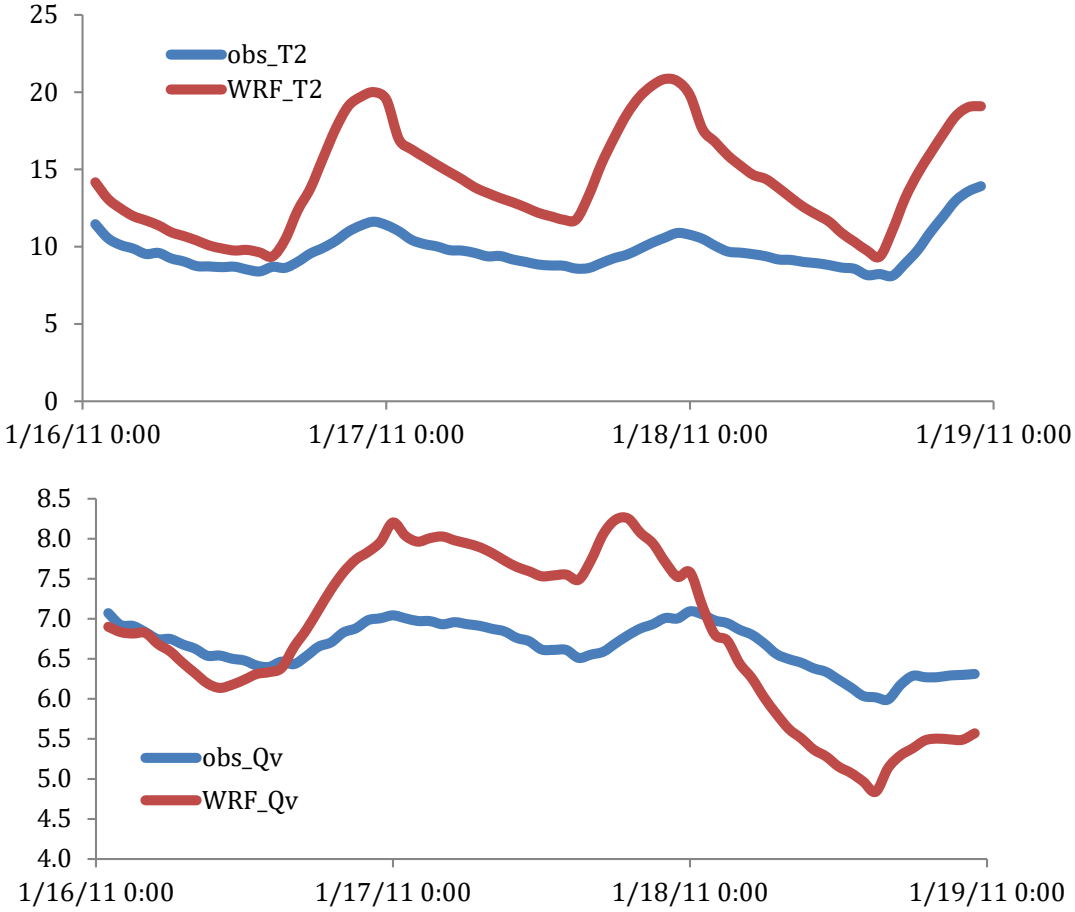

References:

Zhang, H., DeNero, S. P., Joe, D. K., Lee, H.-H., Chen, S.-H., Michalakes, J., and Kleeman, M. J.: Development of a source oriented version of the WRF/Chem model and its application to the California regional PM10 / PM2.5 air quality study, Atmos. Chem. Phys., 14, 485-503, doi:10.5194/acp-14-485-2014, 2014.

2) What is the reason of early dissipation of fog in the model simulations?

Reply: The model under-predicts liquid water path in the middle of the Central Valley, which caused the fog to dissipate earlier (late 17 January). "**Once the surface temperature increases in one area due to thin fog, the dissipation spreads out quickly until the fog completely vanishes."** We have added this explanation in the revised manuscript in Lines 418-419.

3) Which fields are nudged by using FDDA? Temperature and water vapor mixing ratio?

Reply: SOWC model simulations started at 0000 UTC 9 January (7 days prior to the start of the thick fog event) with four-dimensional data assimilation (FDDA)**, which nudges model fields in domain 1 to analysis including the u and v components of horizontal winds, water vapor mixing ratio, and temperature above the PBL height in domain 1 in all simulations.** The bolded texts are added in Lines 376-378.

4) Did you see the same simulation results without KF cumulus scheme in a 4-km inner domain?

Reply: "**No cumulus scheme is used in the most inner domain (4 km resolution).**" It is added in Line 359-360.

5) Please check the following sentence. "aerosol radiative forcing the shortwave energy flux reaching the ground reduces by ~3.7 W m−2 in this case study."

Reply: Modified to **"the shortwave energy flux that reached the ground was reduced by ~3.7 W m^{-2} due to aerosol radiative forcing in this case study"** in Lines 460-461.

6) "S_ARon_CRmod also captured the diurnal pattern of T2 and Q2 during the fog event, but under-predicted the absolute magnitude of T2 and Q2 by 1.76 (2.22) °C and 0.56 (0.88)g kg^{-1} in the daytime (nighttime),..." → Even though the authors showed the bias variation (difference) in Figure 9, it would be better to show the diurnal variation of observation and simulation, respectively.

Reply: To limit the number of figures in the manuscript, we added time series variation of T2, Q2 and NSF from observation, S_ARon_CRmod, S_ARoff_CRmod, and I_ARon_CRmod in the supplementary (Figure S1).

7) Please check the following sentences. “, but S_ARon_CRorig had slightly cloud droplet number concentrations (Table 5).”

Reply: Modified to “**Although S_ARon_CRorig had slightly higher cloud droplet number concentrations, the modified calculation of the cloud optical properties in S_ARon_CRmod gave a similar cloud amount and net shortwave radiation flux reaching the surface, which produced nearly identical feedbacks to meteorology in both experiments (Table 5).**” Please also see Lines 487-490.

Implementation of Warm-Cloud Processes in a Source-Oriented WRF/Chem Model to Study the Effect of Aerosol Mixing State on Fog Formation in the Central Valley of California

Hsiang-He Lee[1*], Shu-Hua Chen[1@], Michael J. Kleeman[2], Hongliang Zhang[2], Steven P. DeNero[2], and David K. Joe[2]

[1] Department of Land, Air, and Water Resources, University of California, Davis, CA

[2] Department of Civil & Environmental Engineering, University of California, Davis, CA

Submitted to

Atmospheric Chemistry and Physics

October 18, 2015

[@]Corresponding author address: Dr. Shu-Hua Chen, Department of Land, Air, and Water Resources, University of California, Davis, California 95616-8627.
E-mail: shachen@ucdavis.edu

*now at: Singapore-MIT Alliance for Research and Technology (SMART), Centre for Environmental Sensing and Modeling (CENSAM), Singapore

Abstract

The source-oriented Weather Research and Forecasting chemistry model (SOWC) was modified to include warm cloud processes and applied to investigate how aerosol mixing states influence fog formation and optical properties in the atmosphere. SOWC tracks a 6-dimensional chemical variable (X, Z, Y, Size Bins, Source Types, Species) through an explicit simulation of atmospheric chemistry and physics. A source-oriented cloud condensation nuclei module was implemented into the SOWC model to simulate warm clouds using the modified two-moment Purdue Lin microphysics scheme. The Goddard shortwave and longwave radiation schemes were modified to interact with source-oriented aerosols and cloud droplets so that aerosol direct and indirect effects could be studied.

The enhanced SOWC model was applied to study a fog event that occurred on 17 January 2011, in the Central Valley of California. Tule fog occurred because an atmospheric river effectively advected high moisture into the Central Valley and nighttime drainage flow brought cold air from mountains into the valley. The SOWC model produced reasonable liquid water path, spatial distribution and duration of fog events. The inclusion of aerosol-radiation interaction only slightly modified simulation results since cloud optical thickness dominated the radiation budget in fog events. The source-oriented mixture representation of particles reduced cloud droplet number relative to the internal mixture approach that artificially coats hydrophobic particles with hygroscopic components. The fraction of aerosols activating into CCN at a supersaturation of 0.5% in the Central Valley decreased from 94% in the internal mixture model to 80% in the source-oriented model. This increased surface energy flux by 3-5 W m^{-2} and surface temperature by as much as 0.25 K in the daytime.

1. Introduction

Atmospheric aerosols are complex mixtures of particles emitted from many different anthropogenic and natural sources suspended in the atmosphere. In contrast to greenhouse gases, aerosols have large spatial and temporal variability in the troposphere because of their short lifetimes (about one week) before coagulation, dry deposition, or wet scavenging processes remove them from the atmosphere (Ramanathan et al., 2001). Aerosol particles can influence human health (McMichael et al., 2006), ecological health (over land and ocean) (Griffin et al., 2001), visible range through the atmosphere (Dick et al., 2000), cloud / precipitation formation (Chen et al., 2008), and the net radiation budget of the earth (IPCC, 2007). Some chemical components of aerosol particles are important to direct radiative forcing of the climate due to their optical properties (Tegen et al., 1996). Particulate sulfate scatters incoming solar radiation, leading to an estimated direct forcing of -0.95 W m^{-2} (Adams et al., 2001). Particulate black carbon strongly absorbs incoming shortwave radiation, which warms the mid-level of the atmosphere but cools the earth's surface (Yang et al., 2009;Koch and Del Genio, 2010). Particulate black carbon also leads to reduce relative humidity and cloud liquid water content (semi-direct effect) in the mid-level atmosphere (Ackerman et al., 2000; Koch and Del Genio, 2010). In addition to these direct effects, Twomey (1974) proposed that aerosols indirectly affect the earth's energy budget due to their ability to serve as cloud condensation nuclei (CCN), which are of great importance in cloud development, especially for warm clouds in the mid-to-high latitudes. Large numbers of CCN produce clouds with a greater number of smaller size cloud droplets (Chen et al., 2008). These smaller cloud droplets raise cloud albedo (the first indirect effect) and also suppress the formation of precipitation and prolong cloud lifetime (the second indirect effect) (Albrecht, 1989). The direct, semi-direct, and indirect effects of aerosol particles modify the energy budgets in the atmosphere and on the surface, with corresponding changes in

atmospheric stability. The 2007 IPCC report (IPCC, 2007) concluded that the net forcing of all aerosols could be either positive or negative in the range from -0.7 W m^{-2} to +0.1 W m^{-2}. The majority of this uncertainty is associated with the semi-direct and indirect effects due to the complexity of aerosol-cloud interactions.

The magnitude of the aerosol semi-direct and indirect effects depends on the number concentration, size, and composition of the atmospheric aerosol particles that act as CCN or ice nuclei (IN) (Lohmann and Feichter, 2005; Chen et al., 2008). Particles with hygroscopic components such as water-soluble ions (Na^+, Cl^-, SO_4^{2-}, NO_3^- etc.) readily act as CCN (Chen and Lamb, 1994). Particles that contain hydrophobic components such as freshly emitted organic carbon or elemental carbon must become coated with hygroscopic material before they will easily serve as CCN (Dusek et al., 2006). This aging process is often parameterized in models (Lesins et al., 2002) but little information is available to describe how the aging timescale should respond to changes in temperature, humidity, oxidant concentrations and/or emissions rates. Mineral dust particles (Motoi, 1951; Georgii and Kleinjung, 1967) commonly have a favorable arrangement of surface structure that allows them to serve as IN. Secondary coatings that condense on mineral dust particles may reduce their ability to serve as IN (Sullivan et al., 2010) but increase their ability to serve as CCN (Li and Shao, 2009). All of these effects point to the importance of the particle mixing state when predicting CCN / IN concentrations.

The standard Weather Research and Forecasting (WRF) model, including the chemistry component (WRF/Chem), permits the simulation of the combined direct, indirect and semi-direct effects of aerosols (Chapman et al., 2009;Fast et al., 2006;Grell et al., 2005). WRF/Chem Version 3.1.1 has sophisticated packages to represent chemistry processes (i.e. gas-phase reaction, gas-to-particle conversion, coagulation, etc.) and aerosol size and

composition (Zaveri et al., 2008;Ackermann et al., 1998;Binkowski and Shankar, 1995;Schell et al., 2001). The Modal Aerosol Dynamics Model for Europe with Secondary Organic Aerosol Model (MADE-SORGAM) and the Model for Simulating Aerosol Interactions and Chemistry (MOSAIC) are commonly used aerosol schemes in the WRF/Chem model. Both schemes have inorganic, organic, and secondary organic aerosols and contain aerosol formation processes including nucleation, condensation, and coagulation. The main difference between MADE-SORGAM and MOSAIC is the representation of aerosol size distributions. MADE-SORGAM uses 3 log-normal modes (Aitken, accumulation and coarse) while MOSAIC uses 4 (or 8) aerosol size sections (bins) from 39 nm to 10 μm, respectively. The details of MADE-SORGAM are described in Binkowski and Shankar (1995), Ackermann et al. (1998), Schell et al. (2001), and Grell et al. (2005) and the details of MOSAIC are given in Zaveri et al. (2008).

As mentioned above, the size, composition, and mixing state of aerosols strongly affect their ability to activate into cloud droplets (Lance et al., 2013;Zaveri et al., 2010). However, most WRF/Chem chemistry packages make a global internal mixing assumption in which all particles within a log-normal mode (MADE-SORGAM) / size bin (MOSAIC scheme) in the same grid cell are instantaneously combined such that they have the same chemical composition. In reality, airborne particles are emitted with unique chemical composition and only become internally mixed over a period of hours to days depending on atmospheric conditions. The instantaneous internal mixing assumption alters the optical and chemical properties of particles in WRF/Chem simulations (Zhang et al., 2014) and therefore has the potential to influence aerosol-cloud interaction (i.e. CCN activation).

The primary goal of this research is to quantify the effect of assumptions about particle mixing state on predicted cloud droplet formation within the WRF/Chem model. Warm

cloud processes in the Purdue Lin scheme (Chen and Sun, 2002) were modified in the Source-Oriented WRF/Chem (SOWC) model to investigate the impact of aerosol mixing state on the characteristics of a fog event in the Central Valley of California. The SOWC model explicitly predicts particle mixing state in the presence of emissions, transport, coagulation, chemical transformation, and deposition. The integration of warm-cloud processes with the source-oriented treatment of particles in the current study provides a more realistic approach to understand how mixing state influences direct, indirect, and semi-indirect effects of anthropogenic aerosols.

This paper is organized as follows: the model description and development of warm cloud processes are introduced in section 2; observational data and numerical experiment design are presented in section 3; results are discussed in section 4; and the summary and discussion are provided in section 5.

2. Model Description and Development

2.1 SOWC

WRF is a compressible, non-hydrostatic regional meteorology model, which uses the Arakawa C grid and terrain-following hydrostatic pressure coordinates. The governing equations of the model are written in flux form and can be solved using a range of solution schemes. In the present study, the Runge-Kutta third-order time scheme was employed and fifth- and third-order advection schemes were chosen for the horizontal and vertical directions, respectively (Skamarock et al., 2008). WRF/Chem simulates trace gas and particle chemical concentrations concurrently with the meteorological fields using the same grid structure, the same advection scheme, and the same physics schemes for sub-grid scale transport (Grell et al., 2005). The SOWC model was developed based on WRF/Chem V3.1.1 with significant modifications throughout the code to enable the use of 6D variables. The

standard WRF/Chem model tracks 3-dimensionial chemistries in a 4-dimensional variable (X, Z, Y, Species). The SOWC model tracks a 6-dimensional chemical variable "AQC" (X, Z, Y, Size Bins, Source Types, Species). Particles emitted from different sources have different sizes and chemical compositions, leading to a source-oriented mixture of particles that age in the atmosphere through coagulation and gas-particle conversion (e.g., condensation and evaporation) processes. Airborne particles in the SOWC model influence meteorological conditions through radiative feedbacks and microphysical processes. The model simultaneously tracks particle mass, number concentration, and radius. The number concentration and radius of different particle size bins from each source type are included as the last two elements in the species dimension. Simulations in this study use 38 chemical species (Table 1) from 5 emissions sources (wood smokes, gasoline, diesel, meat cooking, and other aerosol types) and 8 size bins. The initial particle sizes from emissions are 0.005, 0.1105, 0.221, 0.4415, 0.8835, 1.767, 3.535, and 7.0693 microns. Note that the SOWC model uses moving size bins whose sizes change in response to gas-particle conversion during model simulations. The model conserves aerosol mass concentration throughout the simulation of atmospheric processes including emissions, transport, deposition, coagulation, and condensation/evaporation. The gas-phase species emitted from different sources in each grid cell are not tracked separately in the SOWC model at the present time. In the current study, the initial and boundary conditions of aerosol particles are based on observations from the California Regional Particulate Air Quality Study (CRPAQS) (Ying et al., 2008). The distribution of particle emissions for different bins for every source are calculated using emissions inventories provided by the California Air Resources Board (CARB) along with measured chemical speciation profiles (Ying et al., 2008). Further details of the SOWC model structure and source-oriented chemistry processes are described by Zhang et al. (2014) and Joe et al. (2014).

177 **2.2 Cloud microphysics scheme**

178 The original Purdue Lin microphysics scheme was designed as a one-moment water
179 mass conserved microphysics scheme with five hydrometeors: cloud water, rain, cloud ice,
180 snow, and graupel (Lin et al., 1983;Chen and Sun, 2002). Chapman et al. (2009) added a
181 prognostic treatment of cloud droplet number (Ghan et al., 1997) to the Purdue Lin scheme to
182 make a two-moment treatment of cloud water within WRF/Chem. In our study, a source-
183 oriented CCN module was added to the SOWC model to track size-resolved information
184 about activated CCN from various aerosol sources. A new source-oriented 6D cloud
185 variable, "CLDAQC" (X, Z, Y, Size Bins, Source Types, Species) was added to SOWC to
186 describe source-oriented clouds. Droplet radius and number concentration are once again
187 stored as the last two elements in the species dimension of the CLDAQC variable. In the
188 Purdue Lin scheme, all microphysics processes are parameterized with water mass, except
189 autoconversion. Chapman et al. (2009) added the autoconversion parameterization from Liu
190 et al. (2005) into the Purdue Lin microphysics, which depends on cloud droplet number.
191 Chapman et al. (2009) also specified changes to cloud droplet number proportional to the
192 microphysics process rate of cloud water mass. For example, when 10% cloud water
193 becomes rain water after autoconversion, 10% cloud droplets will be moved at the same time.

194 The continuity equation of the mass-coupled mixing ratio of CLDAQC can be written as
195 follows:

196 $$\frac{\partial CLDAQC}{\partial t} = \nabla \cdot \vec{V} CLDAQC + \nabla \cdot K \nabla CLDAQC + P_{AACT} + S_{micro}, \quad (1)$$

197 where $\vec{V}$ is the 3D wind vector and K is the eddy diffusion coefficient. The first two terms on
198 the right hand side of Eq. (1) are the flux divergence of CLDAQC (transport) and sub-grid
199 eddy mixing, respectively. Figure 1 shows the schematic diagram of the sinks and sources of

CLDAQC in the cloud microphysics processes (P_{AACT} and S_{micro}). Aerosol activation (P_{AACT}) is the main source of CLDAQC. The calculation of aerosol activation is based on a maximum supersaturation determined from a Gaussian spectrum of updraft velocities and aerosol chemistry composition for each size bin (Abdul-Razzak and Ghan, 2002). This parameterization of aerosol activation was implemented in WRF/Chem model (Chapman et al., 2009) and is used in this study. Aerosol activation was calculated each time step. Once the environment reached the critical supersaturation, AQC activated as CCN. Water vapor condenses at a diffusion limited rate to cloud droplets (water molecules transferred from vapor to cloud in Purdue Lin scheme) and particle mass/number is transferred from the interstitial aerosol variable (AQC) to the cloud-borne aerosol variable (CLDAQC). The Purdue Lin microphysics scheme uses a saturation adjustment approach (i.e., it adjusts water vapor to the saturation mixing ratio), so CCN activation is calculated before saturation adjustment. After saturation adjustment, the condensation rate due to vapor diffusion is proportional to particle size (Rogers and Yau, 1989). Results from CCN activation tests at relevant supersaturation are discussed in Section 4.3.

Sinks and sources of CLDAQC (S_{micro}) are based on interactions between a cloud droplet and the other hydrometeors (e.g., ice, rain, snow, and graupel) that can remove water from or add water to CLDAQC. The sinks of cloud water, as well as CLDAQC, include autoconversion from cloud to rain (P_{RAUT}) and the accretion of cloud water by rain (P_{RACW}), snow (P_{SACW}), and graupel (P_{GACW}). The exchange between cloud water and cloud ice can also occur through homogenous freezing of cloud water to ice (P_{IHOM}) and melting of cloud ice to cloud water (P_{IMLT}). Finally, the condensation (associated with P_{ACCT}) and evaporation of cloud water (P_{CEVP}) are implicitly taken into account in the Purdue Lin microphysics scheme. When cloud droplets fully evaporate (sink of CLDAQC), the residual cores are released back into the corresponding source type and size bin of the aerosol (AQC) variable.

225 **2.3 Radiation schemes**

226 The NASA Goddard shortwave and longwave radiation schemes (Chou and Suarez,
227 1999b, 2001b) are used in conjunction with the source-oriented cloud droplet algorithms in
228 the enhanced SOWC model. Absorption of radiation by water vapor, ozone, oxygen, carbon
229 dioxide, cloud droplets and aerosol particles is considered. Interactions among the absorption
230 and scattering by clouds and aerosols (Mie scattering), molecules (Rayleigh scattering) and
231 the surface are fully accounted for (Skamarock et al., 2008). Three main optical parameters
232 are calculated for each model layer to describe the influence of aerosols on the radiation:
233 aerosol optical thickness (τ), single scattering albedo (ω), and asymmetry factor (g). In the
234 present study, the numerical code described by Ying and Kleeman (2003) was implemented
235 to calculate the optical properties of source-oriented particles. The original numerical code
236 of Mie scattering developed by Bohren and Huffman (1983) was used to calculate the particle
237 extinction efficiency, scattering efficiency and asymmetry factor. The partial molar
238 refractive index approach described in Stelson (1990) was used to estimate the mean
239 refractive index for multi-component aerosols. .

240 For any wavelength of shortwave or longwave radiation (λ), the aerosol optical thickness
241 (τ_a) of a model layer with depth h (m) containing a number concentration $n_a(r)$ (# m^{-3} μm^{-1})
242 of droplets with radius r (μm) is given by

243 $$\tau_a(\lambda) = \pi h \int_0^\infty Q_e(\lambda, r) r^2 n_a(r)\, dr, \quad (2)$$

244 where, Q_e is the dimensionless extinction efficiency. The equivalent definition of aerosol
245 optical thickness for discrete size bins j with a mean radius r_j (μm) can be written as

246 $$\tau_a(\lambda) = \pi h \sum_i^n \sum_j^m Q_{ei,j}(\lambda, r) {r_{i,j}}^2 N_{i,j}, \quad (3)$$

where subscript *i* refers to emission source, subscript *j* refers to size, *n* is the number of particle source types and *m* is the number of particle sizes. *N* (# m^{-3}) is the number of particles. The mean asymmetry factor (g_a) and single scattering albedo (ω_a) are calculated using the method described in (Yang, 2000):

$$g_a(\lambda) = \frac{\sum_i^n \sum_j^m Q_{si,j}(\lambda,r) g_{i,j}(\lambda,r) N_{i,j} \pi r_{i,j}^2}{\sum_i^n \sum_j^m Q_{si,j}(\lambda,r) N_{i,j} \pi r_{i,j}^2}, \quad (4)$$

$$\omega_a(\lambda) = \frac{\sum_i^n \sum_j^m Q_{si,j}(\lambda,r) N_{i,j} \pi r_{i,j}^2}{\sum_i^n \sum_j^m Q_{ei,j}(\lambda,r) N_{i,j} \pi r_{i,j}^2}, \quad (5)$$

where Q_s is the dimensionless scattering efficiency. All of the optical parameters are functions of the wavelength (λ) of incident radiation.

In the original Goddard radiation schemes, cloud droplets are assigned to a mono-disperse size distribution (mean effective radius) which depends on the water mass and number concentration. The source-oriented cloud (CLDAQC) contains size distribution and chemistry information which is more realistic than the mono-disperse assumption. Equations 3-5 are applied to all size bins of not only the AQC but also the CLDAQC variables to calculate optical properties and radiative forcing.

3. Numerical experiment designs

3.1 Fog event

A numerical simulation of fog was carried out with the SOWC model as a convenient method to test the effects of particle mixing state on warm clouds processes. The influence of particle size and composition on fog formation and droplet growth has been studied in previous field experiments (Frank et al., 1998;Moore et al., 2004;Ming and Russell, 2004;Cubison et al., 2008;Niu et al., 2012) and modeling studies (Bott and Carmichael, 1993;Kleeman et al., 1997). The results indicate that particle chemical composition and

mixing state strongly influence fog droplet activation, mirroring the processes of interest for cloud droplets.

Tule fogs (radiation fog) frequently form in the Central Valley of California during the winter season (Hayes et al., 1992). Winter in the Central Valley is associated with the maximum concentration of airborne particulate matter (PM) (Chow et al., 1993) which is composed of aerosol particles that can act as CCN. We chose this challenging weather system for the first study of this kind since Tule fog is important in safety, hydrology and agriculture in California. Fog is also an excellent scientific case study that can isolate cloud activation and diffusive growth, the first step of aerosol-cloud-radiation interactions, from other microphysical processes which usually do not occur in fog. In the present study, a thick fog event that occurred on 16 and 17 January 2011 (Fig. 2) was chosen to investigate the impact of source-oriented aerosol-cloud-radiation interactions on fog formation. Fog started forming over the northern Central Valley on 13 January with observed surface relative humidity reaching 95-100% and extended to the southern Central Valley on 14 January. The fog became thicker on 16 January and reached the maximum on 17 January (Fig. 2). This is evident by retrieved cloud optical thickness from MODIS (discussed later). The fog started dissipating from the northern Central Valley on 18 January and fully dissipated on 19 January (Fig. 2c).

In addition to calm wind and radiative cooling, high moisture is an important ingredient to a Tule fog event in the Central Valley, California. Figure 3 shows the time series of column integrated water vapor, sea level pressure, and 850-hPa wind vectors from ECMWF Interim reanalysis data. On 11 January, the column water vapor (CWV) was very low, less than 10 mm, over the Central Valley (Fig. 3a). Moisture was advected into the Central Valley (Fig. 3b) by a winter cyclone moving close to the northwestern coast of the United Sates on 12 January. A weak southwest-northeast-oriented atmospheric river with a width of

1000 km and a maximum CWV of ~26-28 mm approached the western coast and brought moisture into the Central Valley. At 0000 UTC 13 January (Fig 3c), moisture content began increasing in the northern Central Valley. At night, drainage flow from the surrounding mountains brought cold air into the Central Valley, mixed with the low-level moist air, and initiated fog formation over the northern Central Valley. On 14 January (Fig. 3d), the CWV over the southern Central Valley reached 22-24 mm and fog formed over the southern Central Valley.

On 15 and 16 January, a more intense, west-southwest to east-northeast oriented atmospheric river advected moisture into northern California (Figs. 3e and f). The moisture in the Central Valley reached a maximum on 17 January (Fig. 3g), at the time when the fog reached its maximum thickness during the study period (Fig. 2; also see the cloud optical thickness discussion later). On 18 January (Fig. 3h), while high moisture and fog still presented over the southern Central Valley, the moisture decreased and the fog disappeared over the northern Central Valley. Fog fully dissipated in the Central Valley on 19 January.

According to the satellite images and surface temperature variation, the coverage and thickness of fog followed a diurnal pattern with thinning in the daytime and thickening at night. As mentioned earlier, the aerosol mixture state can impact fog formation and properties of cloud droplets.

3.2 Observational data

Multiple types of measurement data were used to evaluate the SOWC model performance. Moderate Resolution Imaging Spectroradiometer (MODIS) level 2 cloud products from the Terra and Aqua satellites provide 5-km resolution cloud optical thickness (COT) and liquid water path (LWP). The LWP retrieval from MODIS has been used to study low cloud and fog (Bendix et al., 2005). High-resolution MODIS data can describe fog spatial distribution and intensity but are only available once every 24 hours (daytime only)

from each satellite. The SOWC model predictions for temperature and moisture at the surface are also evaluated against *in situ* time-series meteorological data from 24 surface weather stations along with net ground shortwave fluxes at 42 sites from California Irrigation Management Information System (CIMIS). Measured concentrations of airborne particles were obtained from the California Ambient Air Quality Data (CAAQD) provided by the Planning & Technical Support Division (PTSD) of the California Air Resources Board (CARB). The station details of CAAQD are provided in Table 2. The locations of all measurement sites are provided in Fig. 4.

3.3 Numerical experiment design

The primary objective of this study is to examine how the source-oriented (S_) and internal (I_) mixture representations of aerosol particles differ in their feedbacks to meteorology in a fog event. Internally mixed simulations (I_) artificially blend emissions from all sources into a single particle size distribution thereby concealing all advanced treatments of particle mixing and aging. Four experiments were carried out (Table 3) for the selected fog event. In the basecase experiment of S_ARon_CRmod, the polluted aerosol particles tracked by AQC act as the source of CCN (S_) and the aerosol-radiation interaction (aerosol direct effect) is enabled in the radiation schemes (ARon). The geometric-optics approach mentioned in Section 2.3 is used to calculate the cloud optical properties of each model layer (CRmod). S_ARon_CRorig is similar to S_ARon_CRmod, except for the use of the original cloud optical property calculation (CRorig) in the NASA Goddard shortwave and longwave radiation schemes. As discussed previously, the original schemes are based on an estimate of the cloud droplet effective radius using the cloud mass and number concentration (CRorig). The radius of cloud droplets in the original Goddard shortwave radiation scheme is constrained to the range from 4 μm to 20 μm. In the modified cloud-radiation scheme (CRmod), the size range of cloud droplets in Eq. (3) can vary between the dry aerosol particle

radius to 30 μm. S_AROff_CRmod has no aerosol direct effect in the radiation schemes (AROff). The comparison of S_AROff_CRmod and S_ARon_CRmod is used to estimate the aerosol direct effect in this study.

Each numerical experiment employed two domains with two-way nesting. Domain 1 (86 x 97 grid cells) had a resolution of 12 km while domain 2 (127 x 202 grid cells) had a resolution of 4 km. Domain 2 was positioned to cover the entire Central Valley of California and results from this domain are used for the subsequent analysis. All simulations used 31 vertically staggered layers based on a terrain-following pressure coordinate system. The vertical layers are stretched with a higher resolution near the surface (an average depth of ~30 m in the first model half layer). Variables other than vertical velocity and geopotential were stored in the half model levels. The time step was 60 seconds for the first domain and 20 seconds for the second domain. The physics schemes employed for the simulations included the modified Purdue Lin microphysics scheme (Chen and Sun, 2002), the NASA Goddard longwave/shortwave radiation schemes (Chou and Suarez, 1999a, 2001a), the Kain-Fritsch cumulus scheme (Kain and Fritsch, 1990;Kain, 1993) (domain 1 only), the YSU PBL scheme (Hong et al., 2006;Hong, 2010) and the Noah LSM surface scheme (Tewari et al., 2007). No cumulus scheme is used in the inner-most domain (4 km resolution). The number of cloud droplets was not considered in the convective scheme in the SOWC model. The target episode had calm winds with local fog formation in the Central Valley (not propagating in through lateral boundaries). Moreover, the event occurred in the winter season when the Convective Available Potential Energy (CAPE) was small. Therefore, the KF cumulus convective parameterization is inactive for this cases study. The meteorological initial and boundary conditions were taken from North American Regional Reanalysis (NARR), which has a spatial resolution of 32 km and a temporal resolution of 3 hours.

The SOWC model tracked two 6D variables for aerosol/cloud properties which introduce considerable computational burden for model simulations when compared to standard WRF/Chem model simulation (with prescribed aerosol concentration). The computational cost of the SOWC model, which is proportional to the extra information that is tracked, is approximately 25 times greater than the standard WRF/Chem 3.1.1 simulation with prescribed aerosols (chem_opt = 0) or approximately 5 times greater than the standard WF/Chem 3.1.1 simulation with any chemistry option (/=0) in the current study. SOWC model simulations started at 0000 UTC 9 January (7 days prior to the start of the thick fog event) with four-dimensional data assimilation (FDDA), which nudges model fields in domain 1 to analysis including the u and v components of horizontal winds, water vapor mixing ratio, and temperature above the PBL height in all simulations. This approach provides a realistic heterogeneous aerosol distribution and low-level temperature and moisture fields at the start of the thick fog simulation. Observations from surface stations and NARR data were used for nudging during this aerosol spin-up period. Between 0000 UTC 16 January to 0000 UTC 19 January, the SOWC model integrated without FDDA (3 day free run) during which time the effects of the different model configurations were observed and is our major interested time period.

Hsiang-He Lee 2/24/2016 4:39 PM
Formatted: Font color: Auto

Hsiang-He Lee 2/24/2016 4:39 PM
Deleted: higher

Hsiang-He Lee 2/24/2016 4:39 PM
Deleted: that of

Hsiang-He Lee 2/24/2016 4:39 PM
Formatted: Font color: Auto

Hsiang-He Lee 2/24/2016 4:39 PM
Formatted: Font color: Auto

Hsiang-He Lee 2/24/2016 4:39 PM
Formatted: Font color: Auto

Hsiang-He Lee 2/24/2016 4:39 PM
Formatted: Font color: Auto

Hsiang-He Lee 2/24/2016 4:39 PM
Deleted:).

4. Model Results

4.1 Evaluation of basecase (S_ARon_CRmod) model performance

The SOWC model calculates CCN number concentrations based on the activation of aerosols (AQC). The AQC number concentration can influence the intensity of initial fog formation and spatial distribution of final fog fields, and thus AQC number concentration is examined first. Figure 5 shows 72-hour averaged (from 16 to 18 January 2011) AQC number concentrations in California's Central Valley that were also averaged over the first five model layers for S_ARon_CRmod. Fog usually forms within the planet boundary layer (PBL),

396 which reaches to a height of approximately five model layers in winter conditions in the
397 Central Valley (450-550 m). Temporally averaged AQC concentrations are approximately
398 2×10^{9} # m^{-3}, with the highest concentrations predicted in the vicinity of polluted cities (e.g.,
399 the San Francisco Bay Area, Stockton, Modesto, Sacramento, Fresno, and Bakersfield), in the
400 middle of the Central Valley, and at foothills of Sierra Nevada Mountain over the east-
401 southeastern Central Valley.

402 Figure 6 shows the comparison of simulated nitrate (NO_3^-), sulfate (SO_4^{2-}), ammonium
403 (NH_4^+) and soluble sodium (Na^+) concentrations to measured values at 6 monitoring stations
404 (see Table 2 and Fig. 4) on 18 January 2011. Simulated sulfate and soluble sodium are in
405 reasonable (>80%) agreement with measurements but nitrate and ammonium concentrations
406 were under predicted by approximately 70%. The cause for this discrepancy is unknown, but
407 one possibility is the presence of organic nitrate compounds in the atmosphere that are not
408 simulated by the model chemistry. Note that both observed and predicted nitrate
409 concentrations in the current episode are lower than the maximum concentrations observed in
410 historical extreme episodes within the San Joaquin Valley (SJV) because the current
411 stagnation event only lasted a few days while extreme events last multiple weeks. If more
412 discussion of aerosol perditions form the SOWC model is desired, we refer the reader to
413 Zhang et al. (2014) who present a comparison of predicted aerosol concentrations and
414 measured concentrations using field campaign data measured during the California Regional
415 PM_{10} / $PM_{2.5}$ Air Quality Study (CRPAQS) in December 2000 – January 2001.

Hsiang-He Lee 2/24/2016 4:39 PM
Deleted:

Hsiang-He Lee 2/24/2016 4:39 PM
Formatted: Font color: Auto

416 The S_ARon_CRmod experiment reasonably reproduces the observed spatial
417 distribution and magnitude of liquid water path (LWP) compared to the data retrieved from
418 MODIS (Fig. 7). In particular, the model predicts LWP well over the northern portion of the
419 Central Valley during the fog event (16 to 18 January). However, the model under-predicts
420 LWP in the middle portion of the Central Valley, which caused the fog to dissipate earlier

(late 17 January). Once the surface temperature increases in one area due to thin fog, the dissipation spreads out quickly until the fog completely evaporates. For the southern portion of the Central Valley, the fog event starts earlier (14 to 15 January) and the model reasonably predicts the onset of the event. But the simulated fog is too dense (figure not shown). In addition, the peak of the simulated fog occurs one day earlier (16 January forecast versus 17 January observed). This timing difference could be caused by the change in the microphysics processes at 0000 UTC 16 January. During the FDDA time period (before 16 January), the one-moment bulk microphysics scheme is used. After the FDDA time period, aerosols start being involved in cloud formation. High Nitrate concentrates in the SJV and enhances aerosol activation due to its high hygroscopicity. This could partially explain why the peak of the LWP occurs on 16 January. The details of aerosol chemical properties are discussed by Zhang et al. (2014).

While simulated LWP is comparable to MODIS retrievals with one day shift (Fig. 7), high CCN concentration and smaller cloud droplets, thus high COTs (Fig. 8), are predicted in the SOWC simulations especially in highly polluted areas. High predicted COT results in cold surface temperature, especially in the southern portion of the Central Valley. Overall, the spatial distribution and magnitude of simulated COT also match the satellite data reasonably (Fig. 8), except for the overestimation of COT over the southeastern Central Valley (Fig. 8b and d).

Mean biases of 2-m temperature (T2), 2-m water vapor mixing ratio (Q2), and surface net downward shortwave radiative flux (NSF) over the entire Central Valley from 16 to 18 January 2011 for S_ARon_CRmod are calculated (Fig. 9). Generally, T2 and Q2 of S_ARon_CRmod are under-predicted by 2 °C and 0.7 g kg^{-1}, respectively. The predicted time variation of T2 and Q2 biases is small in the first one and half days but increases after 1600 UTC 17 January because the predicted fog dissipated in the daytime, different from

observations. Since the predicted fog dissipated, simulated NSF increased and was over-predicted by 13.9 W m^{-2}. Low simulated T2 and Q2, particularly during first one and half days, in S_ARon_CRmod are partially due to over-predictions of the fog formation (i.e., too much condensation leading to depleted water vapor), especially over the southern portion of the Central Valley. Overall, S_ARon_CRmod reasonably forecasted LWP and COT spatial pattern and intensity. S_ARon_CRmod also captured the diurnal pattern of T2 and Q2 during the fog event, but under-predicted the absolute magnitude of T2 and Q2 by 1.76 (2.22) °C and 0.56 (0.88) g kg^{-1} in the daytime (nighttime), respectively.

4.2 Source-oriented aerosol direct and indirect effects

S_AROff_CRmod is designed to test aerosol-radiation feedback and so the comparison between S_AROff_CRmod and S_ARon_CRmod can help quantify the aerosol direct effect in the current study. Table 4 shows that the hourly bias mean and standard deviation from 24 surface stations in the daytime and nighttime of S_AROff_CRmod are similar to, but larger than, results from S_ARon_CRmod for T2 and Q2 at the ground. However, compared to S_ARon_CRmod, the smaller cold bias from S_AROff_CRmod is consistent with its larger net downward shortwave radiative flux (NSF) shown in Tables 4 and 5. Table 5 shows that the average NSF within the entire Central Valley from S_AROff_CRmod is higher than S_ARon_CRmod by 3.7 W m^{-2}, which means that the shortwave energy flux that reached the ground was reduced by ~3.7 W m^{-2} due to aerosol radiative forcing in this case study. The maximum increases of T2 and NSF by the aerosol direct effect occurred on 17 January 2011 (Fig. 9). Table 5 also shows the mean value of cloud water mixing ratio, cloud droplet number, surface skin temperature, latent heat flux and sensible heat flux over the Central Valley during 16 to 18 January 2011. Cloud water mixing ratio and cloud droplet number were averaged within the first five model layers. The aerosol direct effect leads to increases

Hsiang-He Lee 2/24/2016 4:39 PM
Deleted: aerosol radiative forcing

Hsiang-He Lee 2/24/2016 4:39 PM
Deleted: reaching

Hsiang-He Lee 2/24/2016 4:39 PM
Deleted: reduces

474 in the cloud water mass and cloud droplet number by 3.3% and 4.5%, respectively, due to
475 reductions in skin temperature (0.1 K) and net shortwave flux (3.7 W m^{-2}).

476 The modified radiation schemes for cloud optical properties in the S_ARon_CRmod
477 experiment do not have significant feedback on spatially and temporally averaged cloud
478 water mass and cloud droplet number (i.e., compared to S_ARon_CRorig) as shown in Table
479 5. Theoretically, the modified cloud-radiation interaction (i.e., geometric-optics method)
480 used in the COT calculations (S_ARon_CRmod) can predict higher COT which leads to
481 slightly lower net shortwave flux and surface skin temperature, especially in the polluted
482 area. The higher COT predictions are likely caused by differences in the size range of cloud
483 droplets and refractive indexes of cloud water with/without chemical composition in the
484 calculation of cloud radiative properties. As mentioned above, the radius of cloud droplets in
485 the original Goddard shortwave radiation scheme is constrained to the range from 4 μm to 20
486 μm, while in our modified radiation scheme, the cloud droplets are allowed to range in size
487 between the dry aerosol particle radius to 30 μm. The parameterization of cloud optical
488 thickness in the original Goddard radiation scheme assumes that cloud droplets are pure
489 water. The modified scheme recognizes the chemical species in the cloud water and
490 considers these species when calculating the cloud droplet index of refraction. However, in
491 this case study the results of these two experiments (i.e., S_ARon_CRmod and
492 S_ARon_CRorig) were very similar. Because the meteorological conditions of the fog event
493 are calm and stable, the cloud microphysics processes are fairly slow and simple (no rain
494 produced in this case). Although S_ARon_CRorig had slightly higher cloud droplet number
495 concentrations, the modified calculation of the cloud optical properties in S_ARon_CRmod
496 gave a similar cloud amount and net shortwave radiation flux reaching the surface, which
497 produced nearly identical feedbacks to meteorology in both experiments (Table 5).

Hsiang-He Lee 2/24/2016 4:39 PM
Deleted: The size distribution of cloud droplets were virtually identical in the original and modified radiation schemes, but

4.3 Internal mixture versus source-oriented aerosols

The mixing state of chemical components among the atmospheric aerosol particles can potentially play an important role in fog formation. The activation of aerosol particles into cloud droplets depends on the critical super-saturation which in turn depends on particle composition. According to the Köhler equation, increased concentrations of solutes will decrease the critical super-saturation required to activate a particle into a CCN. As mentioned earlier, hydrophobic particles (i.e. black carbon) will more easily serve as CCN once they are coated with hygroscopic material (i.e. sulfate). Increased concentrations of solutes can potentially modify the frequency and severity of fog events in polluted air. In this section, we compare results from S_ARon_CRmod (source-oriented experiment) and I_ARon_CRmod (internally mixed experiment) to investigate the activation change and further meteorological responses between internally mixed and source-oriented aerosols. The internally mixed experiment is conducted by lumping all sources together (i.e., AQC source dimension collapsed to one producing a 5D AQC variable).

It is likely that the ratio of CCN concentration (N_{CCN}) to total aerosol concentration (N_{CN}) will be different for each of the five source types tracked in S_ARon_CRmod since the CCN activation depends on the chemical composition and size of the particles. The highest ratio of N_{CCN}/N_{CN} for S_ARon_CRmod and I_ARon_CRmod is located in the southern Central Valley (Fig. 10) due to higher moisture from the atmospheric river resulting in greater aerosols activation to CCNs and smaller residual aerosol number concentration (see Fig. 5). Over the Central Valley during 16 to 18 January 2011, the ratio of N_{CCN}/N_{CN} for each source type is 12.63%, 15.60%, 14.89%, 16.80% and 20.21% for wood smoke, gasoline, diesel, meat cooking, and others, respectively (averaged within the first five model layers). Wood smoke is typically a major source of aerosol (~38%) in California's Central Valley during winter stagnation events (see Table 6) and the organic carbon in wood smoke is water-

soluble (Dusek et al., 2011) which allows these particles to activate more easily than insoluble particles. However, the majority of the wood smoke particles are located in the smallest size bin, so the ratio of N_{CCN}/N_{CN} for wood smoke is comparable with that of hydrophobic diesel. The source type of "others", which has the highest ratio of N_{CCN}/N_{CN}, is dominated by larger dust particles coated with secondary components such as nitrate and are easier to activate, in contrast to the smaller combustion particles emitted from other tracked sources.

The comparison of the average ratio of N_{CCN}/N_{CN} from the first five model layers between S_ARon_CRmod and I_ARon_CRmod is shown on Fig. 10. The spatial patterns produced by both experiments are similar but I_ARon_CRmod has a higher N_{CCN}/N_{CN} ratio, in particular over the northern two thirds of the Central Valley. The largest differences between N_{CCN}/N_{CN} predicted by S_ARon_CRmod and I_ARon_CRmod occur in regions with large emissions of wood smoke (figure not shown). The ratio of N_{CCN}/N_{CN} for both experiments can reach >30% but the highest N_{CCN}/N_{CN} ratio occurs in relatively less polluted regions. The spatially averaged ratio of N_{CCN}/N_{CN} is 16.65% for S_ARon_CRmod and 27.49% for I_ARon_CRmod within the Central Valley over the period of 16 to 18 January. The CCN concentrations and N_{CCN}/N_{CN} ratios between internally mixed and source-oriented experiments at different super-saturations were calculated to better understand this result. Figure 11a shows the 72-hour averaged CCN concentration at super-saturations of 0.02%, 0.05%, 0.1%, 0.2% and 0.5% and total AQC concentration averaged within the first five model layers. Figure 11b presents corresponding N_{CCN}/N_{CN} ratios at 5 different super-saturations. When the super-saturation is less than or equal to 0.2%, the N_{CCN}/N_{CN} ratio predicted from S_ARon_CRmod is comparable or even slightly higher than that predicted from I_ARon_CRmod. In the S_ARon_CRmod tests, 56% of the particles tracked in the AQC variable (mainly in size bins 2-8) are activated as CCN. When the super-saturation is

551 close to 0.5%, the N_{CCN}/N_{CN} ratio from I_ARon_CRmod can be 15% higher than that of
552 S_ARon_CRmod. Most particles tracked in AQC size bin 1 can activate in the internally
553 mixed experiment; however, in the source-oriented experiment only particles in AQC size bin
554 1 associated with wood smoke and "others" sources activate due to the relatively
555 hydrophobic nature of particles associated with other sources (Table 6). Cubison et al.
556 (2008) analyzed observational CCN and CN data in 2005 from a field campaign in California
557 and found that the average ratio of N_{CCN}/N_{CN} was 18% for a super-saturation value of 0.5%,
558 but their predicted N_{CCN}/N_{CN} ratio based on the internal mixture assumptions could reach to
559 more than 50%. In the source-oriented SOWC model, super-saturation values are typically
560 ~0.2-0.3% with maximum value of 0.5% in some areas. The estimated ratio of N_{CCN}/N_{CN} in
561 the source-oriented model is comparable with observations in Cubison et al. (2008),
562 especially in polluted areas. The temporal variations of mean bias of 2-m temperature (T2),
563 2-m water vapor mixing ratio (Q2), and surface net downward shortwave radiative flux
564 (NSF) between internal versus external aerosol mixture states (I_ARon_CRmod versus
565 S_ARon_CRmod) are similar untill 2000 UTC 17 January. After late 17 January, the bias
566 differences between two experiments are more apparent in the daytime than in the nighttime
567 (Table 4). Compared to I_ARon_CRmod, S_ARon_CRmod reduced bias in T2 by 0.25 K in
568 the daytime but had higher bias in NSF. S_ARon_CRmod did predict improved values of
569 Q2. Based on Fig. 9, we know that the source-oriented and internal aerosol mixing states
570 mainly cause differences in surface temperature in the daytime. Figures 12a and b illustrate
571 the relative change ((internally mixed – source-oriented)/source-oriented * 100%) of
572 averaged (16 - 18 January 2011) cloud water mixing ratio and cloud droplet number,
573 respectively, during the daytime. I_ARon_CRmod predicts cloud water mixing ratios that
574 are 40% higher than values predicted by S_ARon_CRmod over the northern Central Valley
575 (Fig. 12a). The largest relative change in predicted cloud water concentration also occurs in

576 the northern Central Valley near the mountains where fogs are initiated by drainage flow.
577 I_ARon_CRmod predicts higher cloud droplet number (Fig. 12b), with the largest relative
578 increases (~50 - 60%) once again observed in areas near mountains and highly polluted
579 regions with more modest changes of 20~30% over remote regions. Internally mixed
580 aerosols reduce the critical saturation ratio for particles by artificially mixing hygroscopic
581 and hydrophobic components that in turn allows particles to activate more easily.

582 The internally mixed experiment (I_ARon_CRmod) predicts lower daytime averaged
583 surface skin temperature and net downward shortwave flux at ground (Fig. 12c and d)
584 corresponding to the areas with higher cloud water mixing ratio and cloud droplet
585 concentrations (Fig. 12a and b). This result is expected since higher cloud water mixing ratio
586 and cloud droplet concentration will reduce the solar radiation flux on the surface. The
587 reduction of surface skin temperature in the internal mixed experiment is proportional to the
588 change of the net shortwave radiation. Figure 13 shows that the area average of latent heat
589 flux (LH) and sensible heat flux (SH) over the Central Valley in S_ARon_CRmod and the
590 average difference of internally mixed and source-oriented experiments. Higher cloud
591 amount and lower surface temperature are predicted in the internally mixed experiment
592 leading to reduced LH and SH fluxes at ground level compared to the source-oriented
593 experiment. The difference between internally mixed and source-oriented predictions for LH
594 and SH reached 3 W m^{-2} and 5 W m^{-2}, respectively, at noon local time (2200 UTC 17
595 January).

596 Table 7 shows hourly mean bias and root-mean-square-difference between internally
597 mixed (I_ARon_CRmod) and source-oriented (S_ARon_CRmod) experiments for six
598 variables within the Central Valley during 16 to 18 January 2011. The mean bias between
599 these two experiments is 1.19×10^{-2} (g m^{-3}) for cloud water mixing ratio and 6.24×10^{7} (# m^{-3})
600 for cloud droplet number. The direction of these trends is expected since internally mixed

aerosols are easier to activate as CCN. The mean bias between internally mixed and source-oriented experiments is -0.15 (K) for surface skin temperature and -6.02 (W m^{-2}) for net shortwave flux. The mean bias of LH and SH is -0.61 and -0.36 (W m^{-2}), respectively. The root-mean-square-difference between these two experiments is large for each variable, meaning that the difference varies strongly with location (see Fig. 12).

5. Summary and discussion

A warm cloud-aerosol interaction module was implemented into the source-oriented Weather Research and Forecasting model with Chemistry (SOWC) to study the aerosol-cloud-radiation interactions during fog simulations. The source-oriented mixture of aerosols is used to explicitly simulate particle aging processes in the atmosphere rather than instantaneously combining particles into an internal mixture. The SOWC model was used to simulate a fog event in California's Central Valley in January 2011 with seven days of FDDA nudging and three days of free run. Fog formation occurred when high moisture content from an Atmospheric River was advected into the Central Valley and cold drainage flows occurred into the valley at night. The initial tests used 5 emissions sources (wood smoke, gasoline, diesel, meat cooking, and others) with particles from each source consisting of 38 chemical species and 8 size bins, spanning a diameter range from 0.01 to 10 microns. The highest model spatial resolution was 4 km.

Four numerical experiments were conducted to test model performance, meteorological feedbacks from internal and source-oriented aerosols, and the impact of aerosol-cloud-radiation interaction on fog formation. Compared to observations, the SOWC model reasonably predicted fog spatial distribution and duration and environmental meteorological feedbacks. However, the model over-predicted liquid water path and cloud optical thickness, which resulted in cold surface temperature bias. The inclusion of aerosol-radiation interaction reduced net downward shortwave radiative flux by an average of 3.7 W m^{-2} and

daytime surface temperature by 0.1 K. Results that used different treatments for aerosol mixing states were compared, and the important findings are: 1) the fraction of N_{CCN}/N_{CN} at a supersaturation of 0.5% in the Central Valley decreased from 94% in the internal mixture model to 80% in the source-oriented mixture model; 2) due to a smaller number of the CCN concentration in the source-oriented mixture model than in the internal mixture model, cloud water mixing ratio and cloud droplet number decreased 5% and 15%, respectively; and 3) compared to observations, the source-oriented mixture model reduced the cold bias for surface temperature by 0.25 K in the daytime relative to the internal mixture model. The source-oriented mixture representation of particles also provided more reasonable predictions for cloud droplet number and cloud water mass versus observations due to different activation properties than the internal mixture representation of particles. The internal mixture model predicted greater activation of CCN than the source-oriented model due to artificial coating of hydrophobic particles with hygroscopic components.

The SOWC model in this study explicitly calculates primary particle aging over a regional scale for fog formation prediction with two-moment microphysics scheme and aerosol-cloud-radiation interactions. The SOWC model should be a useful tool to study aerosol-cloud-radiation interactions. We are now conducting more numerical studies on different weather systems to explore the full range of responses.

Hsiang-He Lee 2/24/2016 4:39 PM
Deleted: public model

Hsiang-He Lee 2/24/2016 4:39 PM
Deleted: and

Hsiang-He Lee 2/24/2016 4:39 PM
Deleted: predict

Hsiang-He Lee 2/24/2016 4:39 PM
Deleted: effects

Hsiang-He Lee 2/24/2016 4:39 PM
Deleted: climate change on the hydrological cycle and energy budget.

Hsiang-He Lee 2/24/2016 4:39 PM
Formatted: Font:Georgia

Hsiang-He Lee 2/24/2016 4:39 PM
Formatted: Font:Georgia

Hsiang-He Lee 2/24/2016 4:39 PM
Formatted: Font:Georgia

Acknowledgment

The authors would like to acknowledge the WRF and WRF-Chem teams for their efforts on model development. This study was funded by the United States Environmental Protection Agency under Grant No. R833372, NASA Grant No. NNX09AC38G, and NASA High-End Computing (HEC) Program through the NASA Advanced Supercomputing (NAS) Division at Ames Research Center (SMD-13-3895). Although the research described in the article has

been funded by the United States Environmental Protection Agency it has not been subject to the Agency's required peer and policy review and therefore does not necessarily reflect the reviews of the Agency and no official endorsement should be inferred.

References

Abdul-Razzak, H., and Ghan, S. J.: A parameterization of aerosol activation 3. Sectional representation, Journal of Geophysical Research: Atmospheres, 107, AAC 1-1-AAC 1-6, 10.1029/2001jd000483, 2002.

Ackerman, A. S., Toon, O. B., Stevens, D. E., Heymsfield, A. J., Ramanathan, V., and Welton, E. J.: Reduction of Tropical Cloudiness by Soot, Science, 288, 1042-1047, 10.1126/science.288.5468.1042, 2000.

Ackermann, I. J., Hass, H., Memmesheimer, M., Ebel, A., Binkowski, F. S., and Shankar, U.: Modal aerosol dynamics model for Europe: development and first applications, Atmospheric Environment, 32, 2981-2999, http://dx.doi.org/10.1016/S1352-2310(98)00006-5, 1998.

Adams, P. J., Seinfeld, J. H., Koch, D., Mickley, L., and Jacob, D.: General circulation model assessment of direct radiative forcing by the sulfate-nitrate-ammonium-water inorganic aerosol system, Journal of Geophysical Research-Atmospheres, 106, 1097-1111, 10.1029/2000jd900512, 2001.

Albrecht, B. A.: AEROSOLS, CLOUD MICROPHYSICS, AND FRACTIONAL CLOUDINESS, Science, 245, 1227-1230, 10.1126/science.245.4923.1227, 1989.

Bendix, J., Thies, B., Cermak, J., and Nau\ss, T.: Ground fog detection from space based on MODIS daytime data-a feasibility study, Weather and forecasting, 20, 989-1005, 2005.

Binkowski, F. S., and Shankar, U.: The Regional Particulate Matter Model: 1. Model description and preliminary results, Journal of Geophysical Research: Atmospheres, 100, 26191-26209, 10.1029/95jd02093, 1995.

Bohren, C. F., and Huffman, D. R.: Absorption and Scattering of Light by Small Particles, Wiley, New York., 1983.

Bott, A., and Carmichael, G. R.: Multiphase chemistry in a microphysical radiation fog model—A numerical study, Atmospheric Environment. Part A. General Topics, 27, 503-522, http://dx.doi.org/10.1016/0960-1686(93)90208-G, 1993.

Chapman, E. G., Gustafson Jr, W. I., Easter, R. C., Barnard, J. C., Ghan, S. J., Pekour, M. S., and Fast, J. D.: Coupling aerosol-cloud-radiative processes in the WRF-Chem model: Investigating the radiative impact of elevated point sources, Atmos. Chem. Phys., 9, 945-964, 10.5194/acp-9-945-2009, 2009.

Chen, J.-P., and Lamb, D.: Simulation of Cloud Microphysical and Chemical Processes Using a Multicomponent Framework. Part I: Description of the Microphysical Model, Journal of the Atmospheric Sciences, 51, 2613-2630, 1994.

Chen, J.-P., Hazra, A., Shiu, C.-J., Tsai, I.-C., and Lee, H.-H.: Interaction between Aerosols and Clouds: Current Understanding, in: Recent Progress in Atmospheric Sciences: Applicatons to the Asia-Pacific Region, edited by: Liou, K. N., and Chou, M.-D., World Scientific Publishing Co. Pte. Ltd., 231-281, 2008.

Chen, S.-H., and Sun, W. Y.: A one-dimensional time-dependent cloud model, j. Meteor. Soc. Japan, 80, 99-118, 2002.

Chou, M.-D., and Suarez, M. J.: A Solar Radiation Parameterization for Atmospheric Studies NASA Tech. Rep. NASA/TM-1999-10460, 15, 1999a.

Hsiang-He Lee 2/24/2016 4:39 PM
Deleted: . ... [1]

Chou, M.-D., and Suarez, M. J.: A Thermal Infrared Radiation Parameterization for Atmospheric Studies, NASA Tech. Rep. NASA/TM-2001-104606, 19, 2001a.
Chou, M. D., and Suarez, M. J.: A solar radiation parameterization for atmospheric studies., NASA Tech. Rep., 38, 1999b.
Chou, M. D., and Suarez, M. J.: A thermal infrared radiation parameterization for atmospheric studies. , NASA Tech. Rep., 55, 2001b.
Chow, J. C., Watson, J. G., Lowenthal, D. H., Solomon, P. A., Magliano, K. L., Ziman, S. D., and Richards, L. W.: PM10 and PM2.5 Compositions in California's San Joaquin Valley, Aerosol Science and Technology, 18, 105-128, 10.1080/02786829308959588, 1993.
Cubison, M. J., Ervens, B., Feingold, G., Docherty, K. S., Ulbrich, I. M., Shields, L., Prather, K., Hering, S., and Jimenez, J. L.: The influence of chemical composition and mixing state of Los Angeles urban aerosol on CCN number and cloud properties, Atmos. Chem. Phys., 8, 5649-5667, 10.5194/acp-8-5649-2008, 2008.
Dick, W. D., Saxena, P., and McMurry, P. H.: Estimation of water uptake by organic compounds in submicron aerosols measured during the Southeastern Aerosol and Visibility Study, Journal of Geophysical Research: Atmospheres (1984–2012), 105, 1471-1479, 2000.
Dusek, U., Reischl, G. P., and Hitzenberger, R.: CCN Activation of Pure and Coated Carbon Black Particles, Environmental Science & Technology, 40, 1223-1230, 10.1021/es0503478, 2006.
Dusek, U., Frank, G. P., Massling, A., Zeromskiene, K., Iinuma, Y., Schmid, O., Helas, G., Hennig, T., Wiedensohler, A., and Andreae, M. O.: Water uptake by biomass burning aerosol at sub- and supersaturated conditions: closure studies and implications for the role of organics, Atmos. Chem. Phys., 11, 9519-9532, 10.5194/acp-11-9519-2011, 2011.
Fast, J. D., Gustafson, W. I., Easter, R. C., Zaveri, R. A., Barnard, J. C., Chapman, E. G., Grell, G. A., and Peckham, S. E.: Evolution of ozone, particulates, and aerosol direct radiative forcing in the vicinity of Houston using a fully coupled meteorology-chemistry-aerosol model, Journal of Geophysical Research: Atmospheres, 111, D21305, 10.1029/2005jd006721, 2006.
Frank, G., Martinsson, B. G., Cederfelt, S.-I., Berg, O. H., Swietlicki, E., Wendisch, M., Yuskiewicz, B., Heintzenberg, J., Wiedensohler, A., Orsini, D., Stratmann, F., Laj, P., and Ricci, L.: Droplet Formation and Growth in Polluted Fogs, Contri. Atmos. Phys., 71, 65-85, 1998.
Georgii, H. W., and Kleinjung, E.: Relations between the chemical composition of atmospheric aerosol particles and the concentration of natural ice nuclei. , J. Rech. Atmos., 3, 145-156, 1967.
Ghan, S. J., Leung, L. R., Easter, R. C., and Abdul-Razzak, H.: Prediction of cloud droplet number in a general circulation model, Journal of Geophysical Research: Atmospheres, 102, 21777-21794, 10.1029/97jd01810, 1997.
Grell, G. A., Peckham, S. E., Schmitz, R., McKeen, S. A., Frost, G., Skamarock, W. C., and Eder, B.: Fully coupled "online" chemistry within the WRF model, Atmospheric Environment, 39, 6957-6975, http://dx.doi.org/10.1016/j.atmosenv.2005.04.027, 2005.
Griffin, D. W., Kellogg, C. A., and Shinn, E. A.: Dust in the wind: Long range transport of dust in the atmosphere and its implications for global public and ecosystem health, Global Change and Human Health, 2, 20-33, 2001.
Hayes, T. P., Kinney, J. J. R., and Wheeler, N. J. M.: California surface wind climatology, California Air Resources Board, Technical Support Division, Modeling and Meteorology Branch, 1992.

753 Hong, S.-Y., Noh, Y., and Dudhia, J.: A New Vertical Diffusion Package with an Explicit
754 Treatment of Entrainment Processes, Monthly Weather Review, 134, 2318-2341,
755 10.1175/mwr3199.1, 2006.
756 Hong, S.-Y.: A new stable boundary-layer mixing scheme and its impact on the simulated
757 East Asian summer monsoon, Quarterly Journal of the Royal Meteorological Society,
758 136, 1481-1496, 10.1002/qj.665, 2010.
759 IPCC: Climate change 2007-the physical science basis: Working group I contribution to
760 the fourth assessment report of the IPCC, Cambridge University Press, 2007.
761 Joe, D. K., Zhang, H., DeNero, S. P., Lee, H.-H., Chen, S.-H., McDonald, B. C., Harley, R. A.,
762 and Kleeman, M. J.: Implementation of a high-resolution Source-Oriented WRF/Chem
763 model at the Port of Oakland, Atmospheric Environment, 82, 351-363,
764 http://dx.doi.org/10.1016/j.atmosenv.2013.09.055, 2014.
765 Kain, J. S., and Fritsch, J. M.: A one-dimensional entraining/detraining plume model and
766 its application in convective parameterization, Journal of the atmospheric sciences, 47,
767 2784-2802, 1990.
768 Kain, J. S.: Convective parameterization for mesoscale models: The Kain-Fritsch scheme,
769 The representation of cumulus convection in numerical models, Meteor. Monogr, 46,
770 165-170, 1993.
771 Kleeman, M. J., Cass, G. R., and Eldering, A.: Modeling the airborne particle complex as a
772 source-oriented external mixture, Journal of Geophysical Research-Atmospheres, 102,
773 21355-21372, 10.1029/97jd01261, 1997.
774 Koch, D., and Del Genio, A. D.: Black carbon semi-direct effects on cloud cover: review
775 and synthesis, Atmos. Chem. Phys., 10, 7685-7696, 10.5194/acp-10-7685-2010, 2010.
776 Lance, S., Raatikainen, T., Onasch, T. B., Worsnop, D. R., Yu, X. Y., Alexander, M. L.,
777 Stolzenburg, M. R., McMurry, P. H., Smith, J. N., and Nenes, A.: Aerosol mixing state,
778 hygroscopic growth and cloud activation efficiency during MIRAGE 2006, Atmos. Chem.
779 Phys., 13, 5049-5062, 10.5194/acp-13-5049-2013, 2013.
780 Lesins, G., Chylek, P., and Lohmann, U.: A study of internal and external mixing scenarios
781 and its effect on aerosol optical properties and direct radiative forcing, Journal of
782 Geophysical Research-Atmospheres, 107, 10.1029/2001jd000973, 2002.
783 Li, W. J., and Shao, L. Y.: Observation of nitrate coatings on atmospheric mineral dust
784 particles, Atmos. Chem. Phys., 9, 1863-1871, 10.5194/acp-9-1863-2009, 2009.
785 Lin, Y.-L., Farley, R. D., and Orville, H. D.: Bulk Parameterization of the Snow Field in a
786 Cloud Model, Journal of Climate and Applied Meteorology, 22, 1065-1092, 1983.
787 Liu, Y., Daum, P. H., and McGraw, R. L.: Size truncation effect, threshold behavior, and a
788 new type of autoconversion parameterization, Geophysical Research Letters, 32,
789 L11811, 10.1029/2005gl022636, 2005.
790 Lohmann, U., and Feichter, J.: Global indirect aerosol effects: a review, Atmos. Chem.
791 Phys., 5, 715-737, 10.5194/acp-5-715-2005, 2005.
792 McMichael, A. J., Woodruff, R. E., and Hales, S.: Climate change and human health:
793 present and future risks, The Lancet, 367, 859-869, 2006.
794 Ming, Y., and Russell, L. M.: Organic aerosol effects on fog droplet spectra, Journal of
795 Geophysical Research: Atmospheres, 109, D10206, 10.1029/2003jd004427, 2004.
796 Moore, K. F., Sherman, D. E., Reilly, J. E., and Collett, J. L.: Drop size-dependent chemical
797 composition in clouds and fogs. Part I. Observations, Atmospheric Environment, 38,
798 1389-1402, http://dx.doi.org/10.1016/j.atmosenv.2003.12.013, 2004.
799 Motoi, K.: Electron-microscope study of snow crystal nuclei, Journal of Meterology, 8,
800 151-156, 1951.

Niu, S. J., Liu, D. Y., Zhao, L. J., Lu, C. S., Lü, J. J., and Yang, J.: Summary of a 4-Year Fog Field Study in Northern Nanjing, Part 2: Fog Microphysics, Pure and Applied Geophysics, 169, 1137-1155, 10.1007/s00024-011-0344-9, 2012.
Ramanathan, V., Crutzen, P. J., Kiehl, J. T., and Rosenfeld, D.: Atmosphere - Aerosols, climate, and the hydrological cycle, Science, 294, 2119-2124, 10.1126/science.1064034, 2001.
Rogers, R. R., and Yau, M. K.: A Short Course in Cloud Physics, Third ed., Butterworth Heinemann, 1989.
Schell, B., Ackermann, I. J., Hass, H., Binkowski, F. S., and Ebel, A.: Modeling the formation of secondary organic aerosol within a comprehensive air quality model system, Journal of Geophysical Research: Atmospheres (1984–2012), 106, 28275-28293, 2001.
Skamarock, W. C., Klemp, J. B., Dudhia, J., Gill, D. O., Barker, D. M., Duda, M. G., Huang, X.-Y., Wang, W., and Powers, J. G.: A Description of the Advanced Research WRF Version 3, NCAR Technical Note, NCAR/TN-475+STR, 2008.
Stelson, A. W.: Urban aerosol refractive index prediction by partial molar refraction approach, Environmental Science & Technology, 24, 1676-1679, 10.1021/es00081a008, 1990.
Sullivan, R. C., Petters, M. D., DeMott, P. J., Kreidenweis, S. M., Wex, H., Niedermeier, D., Hartmann, S., Clauss, T., Stratmann, F., Reitz, P., Schneider, J., and Sierau, B.: Irreversible loss of ice nucleation active sites in mineral dust particles caused by sulphuric acid condensation, Atmospheric Chemistry and Physics, 10, 11471-11487, 10.5194/acp-10-11471-2010, 2010.
Tegen, I., Lacis, A. A., and Fung, I.: The influence on climate forcing of mineral aerosols from disturbed soils, Nature, 380, 419-422, 10.1038/380419a0, 1996.
Tewari, M., Chen, F., Kusaka, H., and Miao, S.: Coupled WRF/Unified Noah/urban-canopy modeling system, NCAR WRF Documentation, NCAR, Boulder, 1-22, 2007.
Twomey, S.: POLLUTION AND PLANETARY ALBEDO, Atmospheric Environment, 8, 1251-1256, 10.1016/0004-6981(74)90004-3, 1974.
Yang, F.: Radiative forcing and climate impact of the Mount Pinatubo volcanic eruption. , PhD, University of Illinois at Urbana-Champaign., 2000.
Yang, M., Howell, S. G., Zhuang, J., and Huebert, B. J.: Attribution of aerosol light absorption to black carbon, brown carbon, and dust in China – interpretations of atmospheric measurements during EAST-AIRE, Atmos. Chem. Phys., 9, 2035-2050, 10.5194/acp-9-2035-2009, 2009.
Ying, Q., and Kleeman, M. J.: Effects of aerosol UV extinction on the formation of ozone and secondary particulate matter, Atmospheric Environment, 37, 5047-5068, 2003.
Ying, Q., Lu, J., Allen, P., Livingstone, P., Kaduwela, A., and Kleeman, M.: Modeling air quality during the California Regional PM10/PM2.5 Air Quality Study (CRPAQS) using the UCD/CIT source-oriented air quality model - Part I. Base case model results, Atmospheric Environment, 42, 8954-8966, DOI 10.1016/j.atmosenv.2008.05.064, 2008.
Zaveri, R. A., Easter, R. C., Fast, J. D., and Peters, L. K.: Model for Simulating Aerosol Interactions and Chemistry (MOSAIC), Journal of Geophysical Research: Atmospheres, 113, D13204, 10.1029/2007jd008782, 2008.
Zaveri, R. A., Barnard, J. C., Easter, R. C., Riemer, N., and West, M.: Particle-resolved simulation of aerosol size, composition, mixing state, and the associated optical and cloud condensation nuclei activation properties in an evolving urban plume, Journal of Geophysical Research: Atmospheres, 115, D17210, 10.1029/2009jd013616, 2010.
Zhang, H., DeNero, S. P., Joe, D. K., Lee, H. H., Chen, S. H., Michalakes, J., and Kleeman, M. J.: Development of a source oriented version of the WRF/Chem model and its

application to the California regional PM10 / PM2.5 air quality study, Atmos. Chem. Phys., 14, 485-503, 10.5194/acp-14-485-2014, 2014.

Captions of Tables

Table 1. Chemical species that are carried in the AQC/CLDAQC "species" dimension. All species are in concentrations (μg m^{-3}) except for the last two elements (i.e., 39 and 40), which carry the number concentration (# m^{-3}) and radius (m).

Table 2. California Ambient Air Quality Data (CAAQD) station information.

Table 3. Numerical experiment designs for this study.

Table 4. Hourly bias mean and standard deviation (std) in day time and night time of 2-m temperature (T2, °C), water vapor mixing ratio (Q2, g kg-air^{-1}), and net downward shortwave radiative flux (NSF, W m^{-2}) between all experiments and observation from 16 to 18 January 2011. T2 and Q2 are calculated using 24 surface stations and NSF is calculated using 42 CIMIS stations shown in Fig. 4.

Hsiang-He Lee 2/24/2016 4:39 PM
Deleted: 10-m wind speed (WSD, m sec^{-1}),

Table 5. Mean values of cloud water mixing ratio (Q_c), cloud droplet number (Q_n), surface skin temperature (SKT), net shortwave flux (NSF), latent heat flux (LH) and sensible heat flux (SH) for four experiments over the entire Central Valley during 16 to 18 January 2011.

Table 6. Ratio of AQC number concentration for each bin/source averaged within the first five model layers during 16 to 18 January 2011.

Table 7. Hourly bias mean and root-mean-square-difference of cloud water mixing ratio (Q_c), cloud droplet number (Q_n), surface skin temperature (SKT), net shortwave flux (NSF), latent heat flux (LH) and sensible heat flux (SH) between internally mixed (I_ARon_CRmod) and source-oriented (S_ARon_CRmod) experiments (internally mixed – source-oriented) during 16 to 18 January 2011.

881 **Captions of Figures**

882 Figure 1. Cloud physics processes that are involved with cloud particles in the SOWC model
883 with a 6D aerosol variable (AQC) and a 6D cloud variable (CLDAQC) included.
884 Black solid arrow and grey dashed arrow indicate the source and the sink processes of
885 cloud water and 6D CLDAQC, as well as 6D AQC, respectively.

886 Figure 2. MODIS true color image at (a) 1930 UTC 16 January 2011 and (b) 1835 UTC 17
887 January 2011 from Satellite Terra, respectively.

888 Figure 3. The column integrated water vapor (shaded; mm), 850-hPa wind vector, and seal
889 level pressure (contours; hPa) from ECMWF Interim reanalysis at (a) 0000 UTC (4
890 pm local time) 11 January, (b) 0000 UTC 12 January, (c) 0000 UTC 13 January, (d)
891 0000 UTC 14 January, (e) 0000 UTC 15 January, (f) 0000 UTC 16 January, (g) 0000
892 UTC 17 January, and (h) 0000 UTC 18 January, 2011.

893 Figure 4. NOAA's National Climatic Data Center (NCDC; 24 stations, red dots), California
894 Irrigation Management Information System (CIMIS; 42 stations, black dots) and
895 California Ambient Air Quality Data (6 stations, numbers corresponding to Table 2
896 station ID) measurement locations. Shaded is terrain height in m.

897 Figure 5. The 72-hour averaged (16 to 18 January 2011) AQC number concentration
898 averaged over the first five model layers from the polluted experiment
899 (S_ARon_CRmod) in units of 10^8 # m^{-3}. Contours are terrain heights in m.

900 Figure 6. Comparison of (a) Nitrate (NO_3^-), (b) Sulfate (SO_4^{2-}), (c) Ammonium (NH_4^+), and
901 (d) Soluble Sodium (Na^+) between simulated source-oriented experiment
902 (S_ARon_CRmod), internally mixed experiment (I_ARon_CRmod) and the observed
903 concentrations of airborne particles on 18 January 2011. Units are μg m^{-3}.

904 Figure 7. Liquid water path (LWP) (g m^{-2}) from MODIS Level 2 cloud products ((a), (c) and

(e)) and from the SOWC model with aerosol feedback on and modified cloud-radiation scheme (S_ARon_CRmod; (b), (d) and (e)). (a) and (b) are at 1900 UTC 16 January 2011. (c) and (d) are at 1800 UTC 17 January 2011. (e) and (f) are at 1900 UTC 18 January 2011. Contours in (b), (d) and (e) are terrain heights in m.

Figure 8. Same as Figure 5 but cloud optical thickness (COT) (dimensionless).

Figure 9. Mean bias variation of (a) 2-m temperature (T2), (b) 2-m water vapor mixing ratio (Q2), and (c) surface net downward shortwave radiative flux (NSF) between observations and model simulation from 16 to 18 January 2011 for S_ARon_CRmod (blue lines), S_ARoff_CRmod (purple lines) and I_ARon_CRmod (red lines) experiments.

Figure 10. N_{CCN}/N_{CN} ratio for (a) S_ARon_CRmod (source-oriented experiment) and (b) I_ARon_CRmod (internally mixed experiment) averaged within the first five model layers. The ratio is hourly average during 16 to 18 January 2011. Contours are terrain heights in m.

Figure 11. (a) 72-hour averaged CCN concentration at supersaturation of 0.02%, 0.05%, 0.1%, 0.2%, 0.5% and total AQC concentration with units in # cm^{-3}. (b) N_{CCN}/N_{CN} ratio at 5 corresponding supersaturation. Dark gray is source-oriented experiment and light gray represents internally mixed experiment. Results are average values using data within the first five model layers.

Figure 12. Relative change ((internally mixed – source-oriented)/source-oriented * 100%) in 72-hour averaged predictions during 16 to 18 January 2011 for (a) the ratio of cloud water mixing ratio, (b) cloud droplet number, (c) surface skin temperature and (d) net shortwave radiation. (a) and (b) are average values using data within the first five model layers. Contours are terrain heights in m.

Figure 13. Area average of latent heat flux (LH) and sensible heat flux (SH) over the Central

930 Valley in S_ARon_CRmod and the average difference between I_ARon_CRmod and
931 S_ARon_CRmod from 0800 UTC 17 January (00 Z local time) to 0700 UTC 18 January
932 (23 Z local time).

933

934

Table 1. Chemical species that are carried in the AQC/CLDAQC "species" dimension. All species are in concentrations (μg m^{-3}) except for the last two elements (i.e., 39 and 40), which carry the number concentration (# m^{-3}) and radius (m).

	Chemical species		Chemical species
1	EC	21	SOA from lumped Alkane 1
2	OC	22	SOA from lumped Alkane 2
3	NA	23	SOA from lumped Aromatic 1
4	CL	24	SOA from lumped Aromatic 2
5	N3	25	SOA from lumped Aromatic 1
6	S6	26	SOA from lumped Aromatic 2
7	N5	27	SOA from lumped Aromatic 1
8	Other	28	SOA from lumped Aromatic 2
9	Metal	29	SOA from lumped Alkene 1
10	Unknown	30	SOA from lumped Alkene 2
11	CU1	31	SOA from lumped Alpha Pinene 1
12	CU2	32	SOA from lumped Alpha Pinene 2
13	MN2	33	SOA from lumped Beta Pinene 1
14	MN3	34	SOA from lumped Beta Pinene 2
15	FE2	35	SOA from lumped Toluene 1
16	FE3	36	SOA from lumped Toluene 2
17	S4	37	Hydrogen Ion
18	Air (hollow sea salt particles)	38	Water
19	NO3	39	Number Concentration
20	Non-explicit SOA	40	Particle Mean Volume Radius

942

943

944

945

946 Table 2. California Ambient Air Quality Data (CAAQD) station information

Station ID	Station name	Longitude (°)	Latitude (°)
1	San Jose-Jackson Street	-121.89	37.35
2	Bakersfield-5558 Cal. Avenue	-119.06	35.36
3	Fresno-1st Street	-119.77	36.78
4	Modesto-14th Street	-120.99	37.64
5	Visalia-N Church Street	-119.29	36.33
6	Sacramento-T Street	-121.49	38.57

947

948 Table 3. Numerical experiment designs for this study.

Experiments	Description
S_ARon_CRmod	Source-Oriented aerosols with aerosol direct effect calculation on and modified cloud radiation parameterization
S_ARon_CRorig	Source-Oriented aerosols with aerosol direct effect calculation on and original cloud radiation parameterization
S_AROff_CRmod	Source-Oriented aerosols with aerosol direct effect calculation off and modified cloud radiation parameterization
I_ARon_CRmod	Internal mixing aerosols with aerosol direct effect calculation on and modified cloud radiation parameterization

949

Table 4. Hourly bias mean and standard deviation (std) in day time and night time of 2-m temperature (T2, °C), water vapor mixing ratio (Q2, g kg-air^{-1}), and net downward shortwave radiative flux (NSF, W m^{-2}) between all experiments and observation from 16 to 18 January 2011. T2 and Q2 are calculated using 24 surface stations and NSF is calculated using 42 CIMIS stations shown in Fig. 4.

	S_ARon_CRmod		S_ARon_CRorig		S_ARoff_CRmod		I_ARon_CRmod	
Daytime	Bias mean	std	Bias mean	std	Bias mean	std	Bias mean	std
T2	-1.76	1.27	-1.72	1.32	-1.63	1.33	-2.01	1.09
Q2	-0.56	0.34	-0.56	0.36	-0.54	0.35	-0.57	0.32
NSF	13.91	53.18	14.40	58.00	18.81	58.78	8.68	50.03
Nighttime	Bias mean	std	Bias mean	std	Bias mean	std	Bias mean	std
T2	-2.22	0.92	-2.21	0.95	-2.19	0.93	-2.30	0.87
Q2	-0.88	0.41	-0.87	0.42	-0.88	0.42	-0.89	0.41
NSF	/	/	/	/	/	/	/	/

Hsiang-He Lee 2/24/2016 4:39 PM
Deleted: $^{-1}$), 10-m wind speed (WSD, m sec

Hsiang-He Lee 2/24/2016 4:39 PM
Formatted: Font color: Black

Table 5. Mean values of cloud water mixing ratio (Q_c), cloud droplet number (Q_n), surface skin temperature (SKT), net shortwave flux (NSF), latent heat flux (LH) and sensible heat flux (SH) for four experiments over the entire Central Valley during 16 to 18 January 2011.

	S_ARon_CRmod	S_ARon_CRorig	S_ARoff_CRmod	I_ARon_CRmod
Q_c* (g m^{-3})	0.220	0.221	0.213	0.231
Q_n* (# m^{-3})	3.94×10^8	4.18×10^8	3.77×10^8	4.57×10^8
SKT (K)	281.305	281.30	281.404	281.151
NSF (W m^{-2})**	130.56	131.02	134.24	124.54
LH (W m^{-2})	9.01	9.02	9.36	8.40
SH (W m^{-2})	4.91	4.55	5.27	4.54
COT (unitless)	25.56	25.15	24.49	28.62

* Averaged within the first five model layers

** Averaged only in the daytime

Hsiang-He Lee 2/24/2016 4:39 PM
Formatted Table

965

966 Table 6. Ratio of AQC number concentration for each bin/source averaged within the first
967 five model layers during 16 to 18 January 2011.

	Wood smoke	Gasoline	Diesel	Meat cooking	Others	Source-oriented	Internal
Bin1	28.92%	1.00%	4.25%	0.84%	10.39%	45.40%	48.89%
Bin2	9.12%	0.38%	1.48%	0.60%	38.64%	50.22%	46.74%
Bin3	0.19%	0.01%	0.03%	0.02%	3.03%	3.28%	3.26%
Bin4	0.00%	0.00%	0.00%	0.00%	0.17%	0.18%	0.21%
Bin5	0.00%	0.00%	0.00%	0.00%	0.02%	0.02%	0.02%
Bin6	0.00%	0.00%	0.00%	0.00%	0.00%	0.00%	0.00%
Bin7	0.00%	0.00%	0.00%	0.00%	0.00%	0.00%	0.00%
Bin8	0.00%	0.00%	0.00%	0.00%	0.91%	0.91%	0.88%

968

Table 7. Hourly bias mean and root-mean-square-difference of cloud water mixing ratio (Q_c), cloud droplet number (Q_n), surface skin temperature (SKT), net shortwave flux (NSF), latent heat flux (LH) and sensible heat flux (SH) between internally mixed (I_ARon_CRmod) and source-oriented (S_ARon_CRmod) experiments (internally mixed – source-oriented) during 16 to 18 January 2011.

	Bias mean	**Root-mean-square-difference**
Q_c^* (g m^{-3})	1.19×10^{-2}	4.16×10^{-2}
Q_n^* (# m^{-3})	6.24×10^{7}	2.64×10^{8}
SKT (K)	-0.15	0.57
NSF (W m^{-2})	-6.02	13.30
LH (W m^{-2})	-0.61	2.75
SH (W m^{-2})	-0.36	5.24

* Averaged within the first five model layers

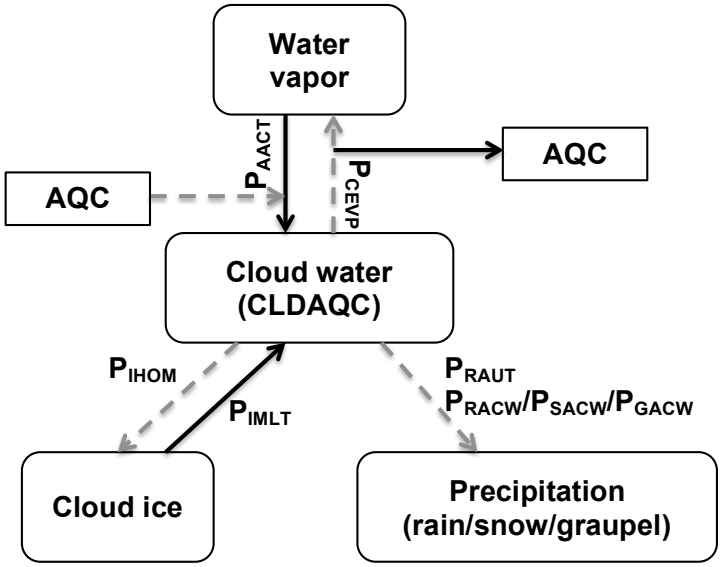

Figure 1. Cloud physics processes that are involved with cloud particles in the SOWC model with a 6D aerosol variable (AQC) and a 6D cloud variable (CLDAQC) included. Black solid arrow and grey dashed arrow indicate the source and the sink processes of cloud water and 6D CLDAQC, as well as 6D AQC, respectively.

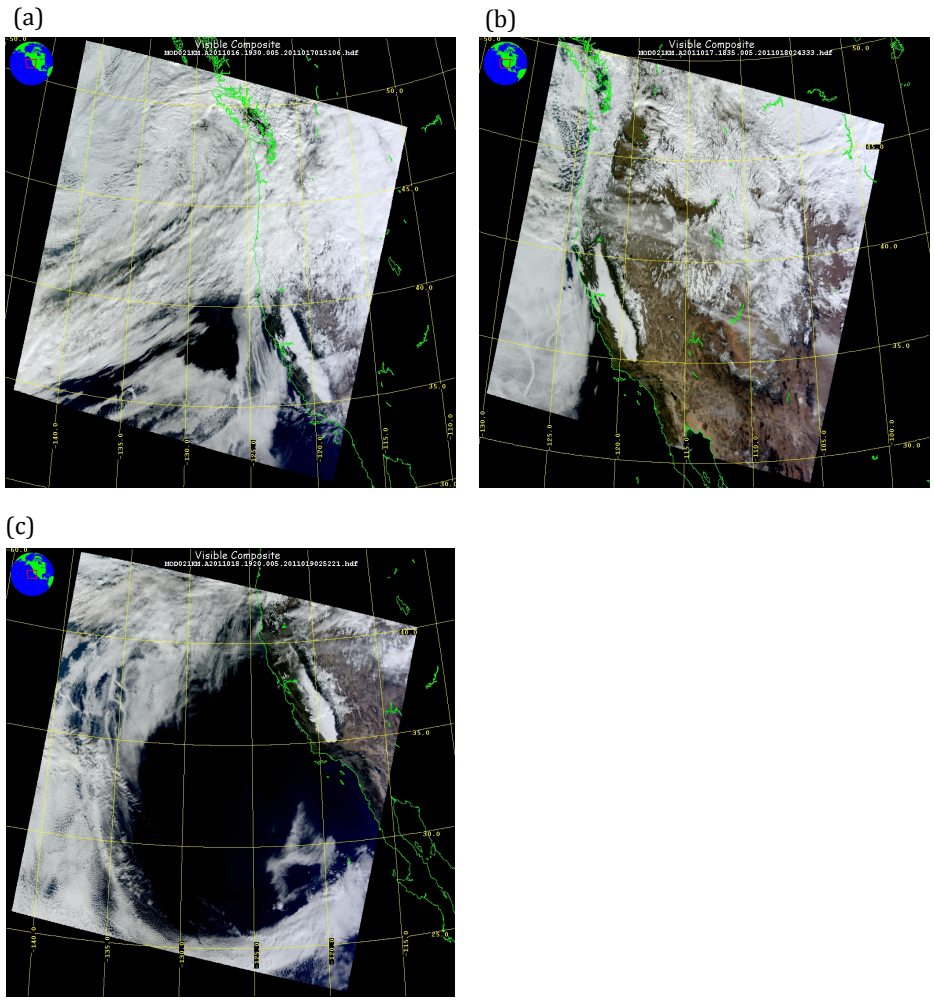

Figure 2. MODIS true color images at (a) 1930 UTC 16 January, (b) 1835 UTC 17 January, and (c) 1920 UTC 18 January, 2011 from Satellite Terra.

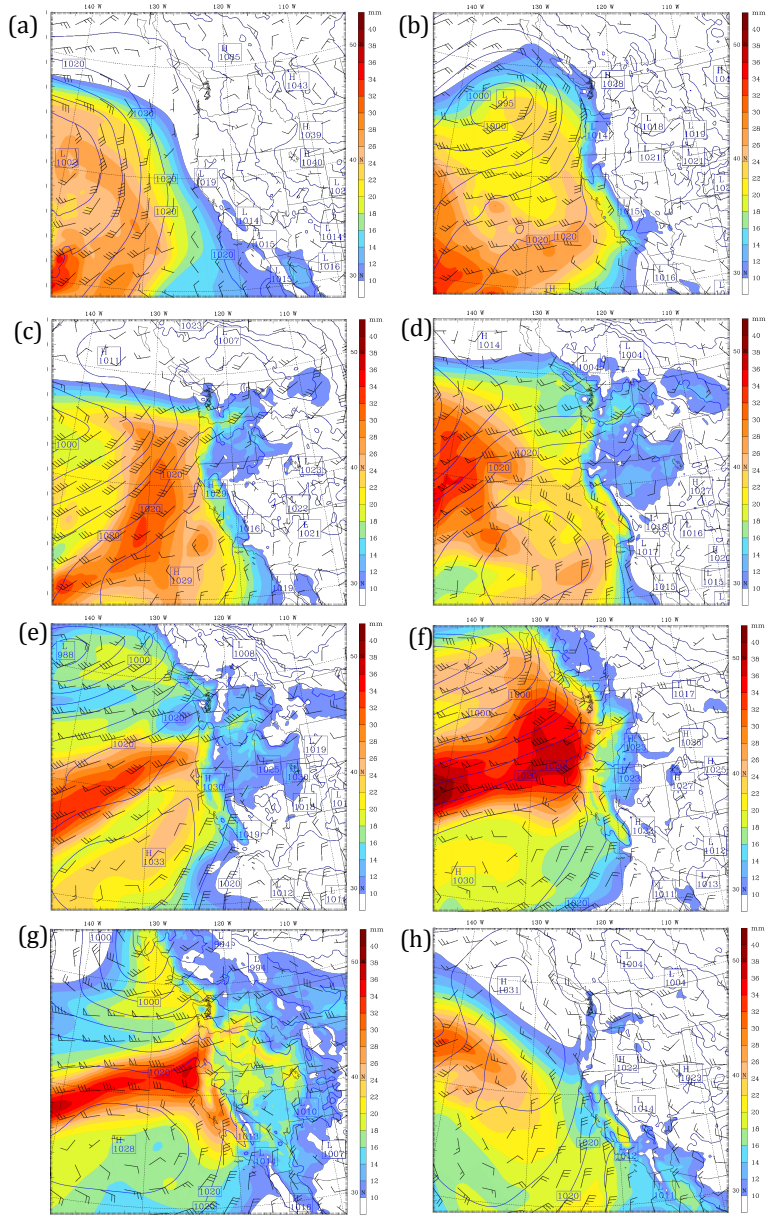

Figure 3. The column integrated water vapor (shaded; mm), 850-hPa wind vector, and sea level pressure (contours; hPa) from ECMWF Interim reanalysis at (a) 0000 UTC (4 pm local time) 11 January, (b) 0000 UTC 12 January, (c) 0000 UTC 13 January, (d) 0000 UTC 14 January, (e) 0000 UTC 15 January, (f) 0000 UTC 16 January, (g) 0000 UTC 17 January, and (h) 0000 UTC 18 January, 2011.

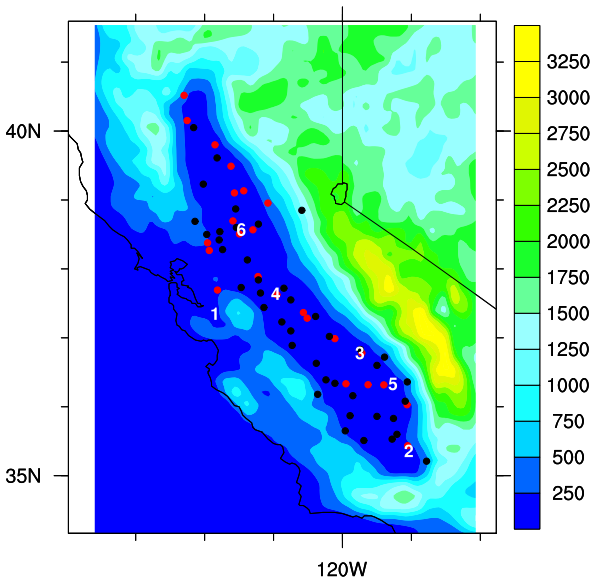

Figure 4. NOAA's National Climatic Data Center (NCDC; 24 stations, red dots), California Irrigation Management Information System (CIMIS; 42 stations, black dots) and California Ambient Air Quality Data (6 stations, numbers corresponding to Table 2 station ID) measurement locations. Shaded is terrain height in m.

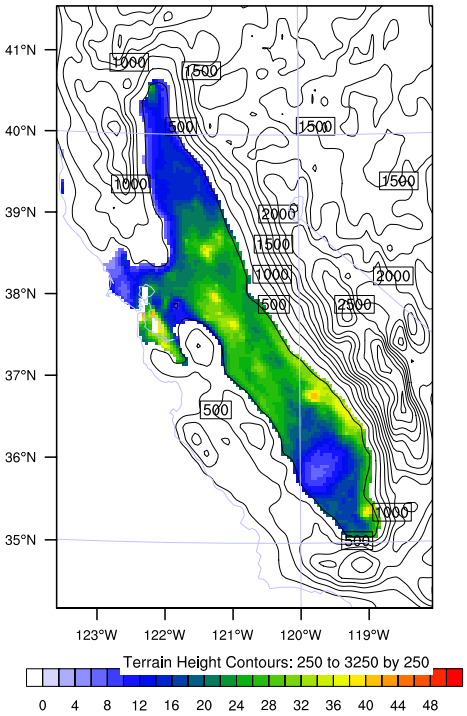

Figure 5. The 72-hour averaged (16 to 18 January 2011) AQC number concentration averaged over the first five model layers from the experiment S_ARon_CRmod in units of 10^8 # m^{-3}. Contours are terrain heights in m.

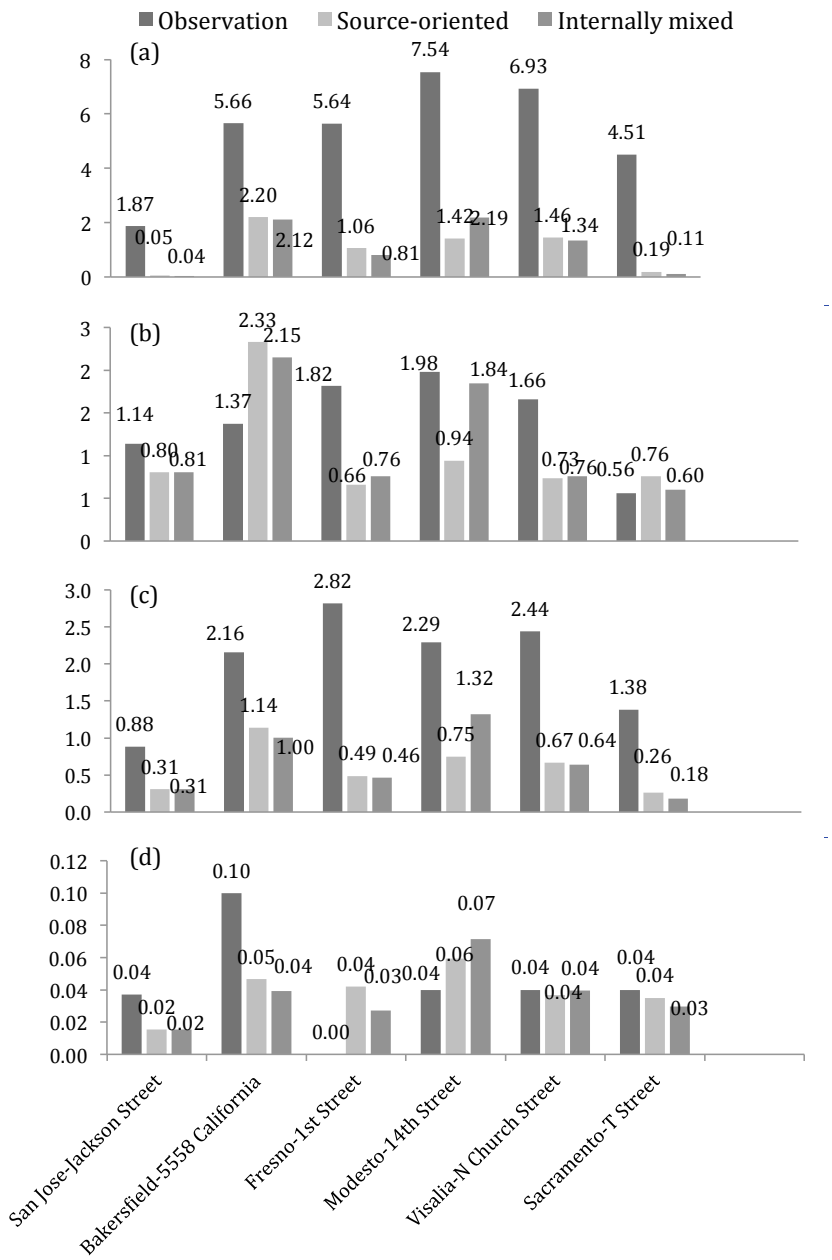

Figure 6. Comparison of (a) Nitrate (NO_3^-), (b) Sulfate (SO_4^{2-}), (c) Ammonium (NH_4^+), and (d) Soluble Sodium (Na^+) between simulated source-oriented experiment (S_ARon_CRmod), internally mixed experiment (I_ARon_CRmod) and the observed concentrations of airborne particles on 18 January 2011. Units are μg m^{-3}.

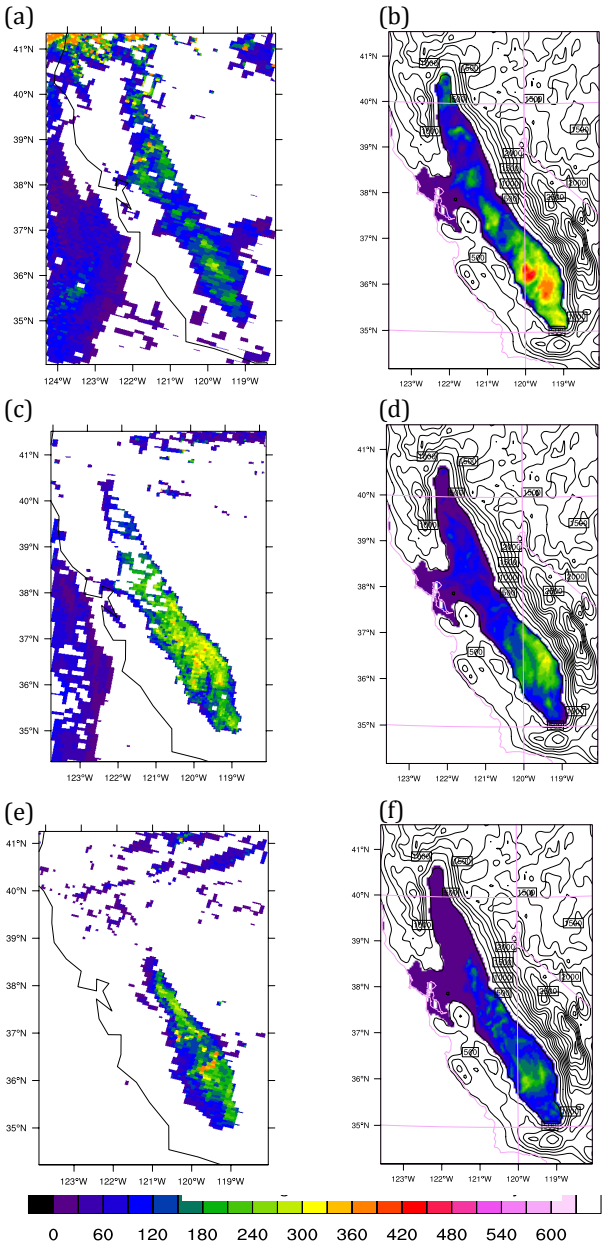

Figure 7. Liquid water path (LWP) (g m^{-2}) from MODIS Level 2 cloud products ((a), (c) and (e)) and from the SOWC model with aerosol feedback on and modified cloud-radiation scheme (S_ARon_CRmod; (b), (d) and (e)). (a) and (b) are at 1900 UTC 16 January 2011. (c) and (d) are at 1800 UTC 17 January 2011. (e) and (f) are at 1900 UTC 18 January 2011. Contours in (b), (d) and (e) are terrain heights in m.

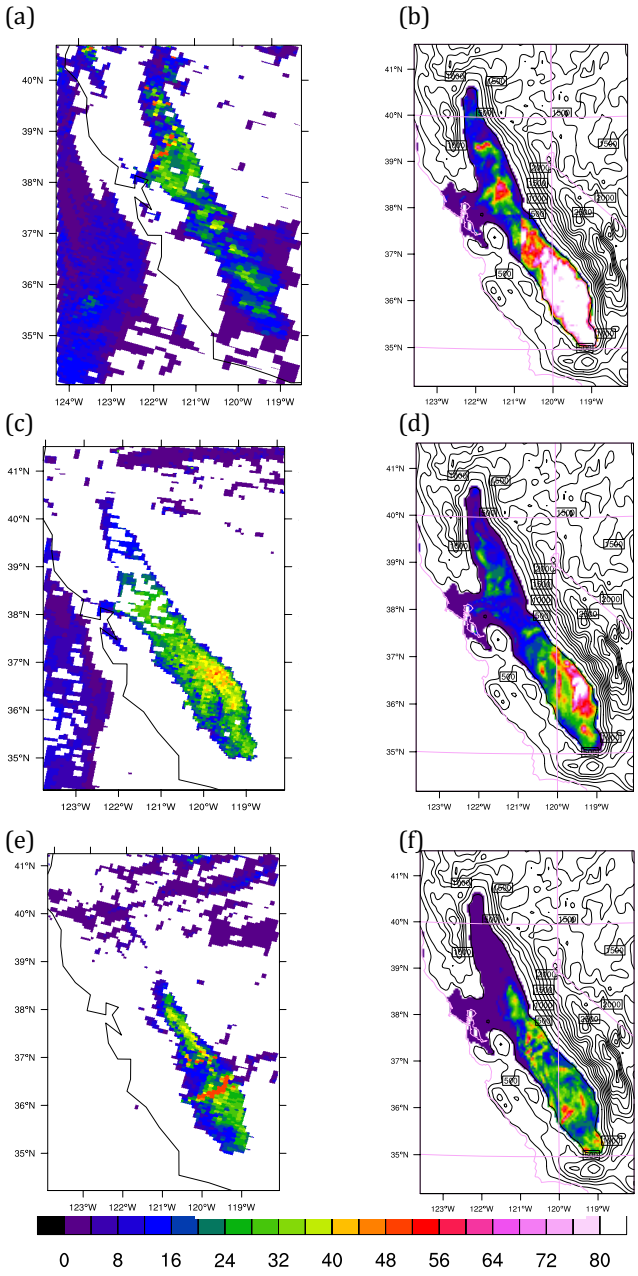

Figure 8. Same as Figure 5 but cloud optical thickness (COT) (dimensionless).

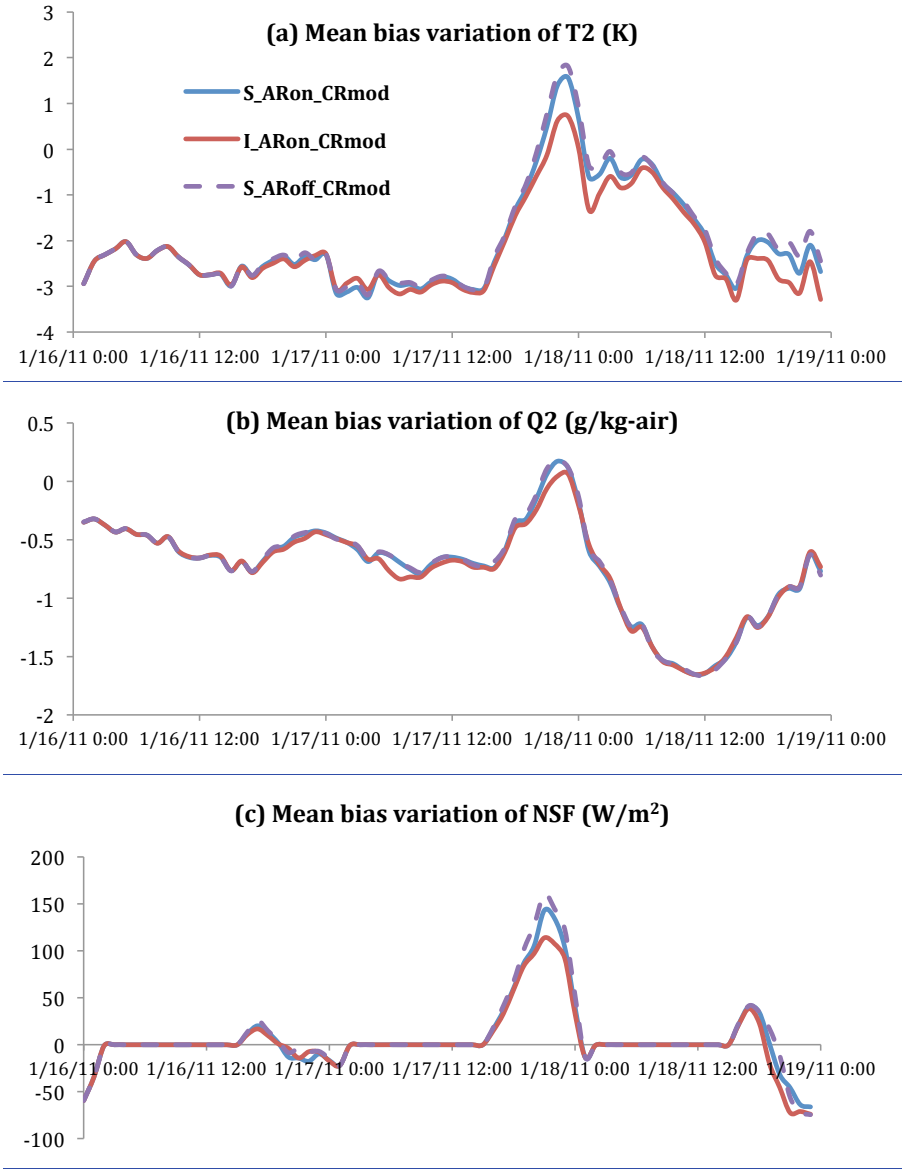

Figure 9. Mean bias variation of (a) 2-m temperature (T2), (b) 2-m water vapor mixing ratio (Q2), and (c) surface net downward shortwave radiative flux (NSF) between observations and model simulation from 16 to 18 January 2011 for S_ARon_CRmod (blue lines), S_ARoff_CRmod (purple lines) and I_ARon_CRmod (red lines) experiments.

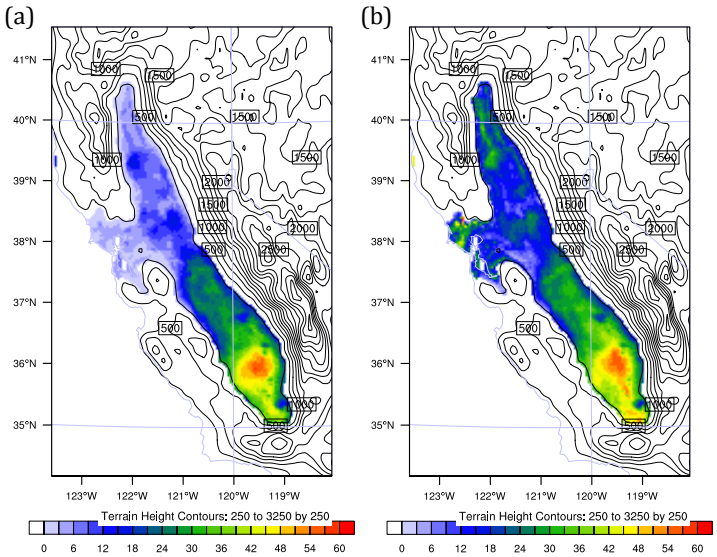

Figure 10. N_{CCN}/N_{CN} ratio for (a) S_ARon_CRmod (source-oriented experiment) and (b) I_ARon_CRmod (internally mixed experiment) averaged within the first five model layers. The ratio is hourly average during 16 to 18 January 2011. Contours are terrain heights in m.

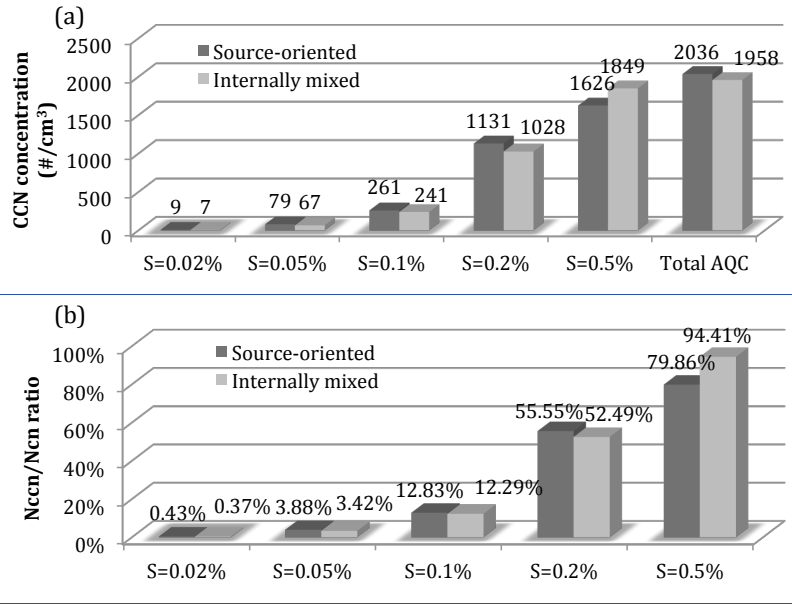

Figure 11. (a) 72-hour averaged CCN concentration at supersaturation of 0.02%, 0.05%, 0.1%, 0.2%, 0.5% and total AQC concentration with units in # cm^{-3}. (b) N_{CCN}/N_{CN} ratio at 5 corresponding supersaturation. Dark gray is source-oriented experiment and light gray represents internally mixed experiment. Results are average values using data within the first five model layers.

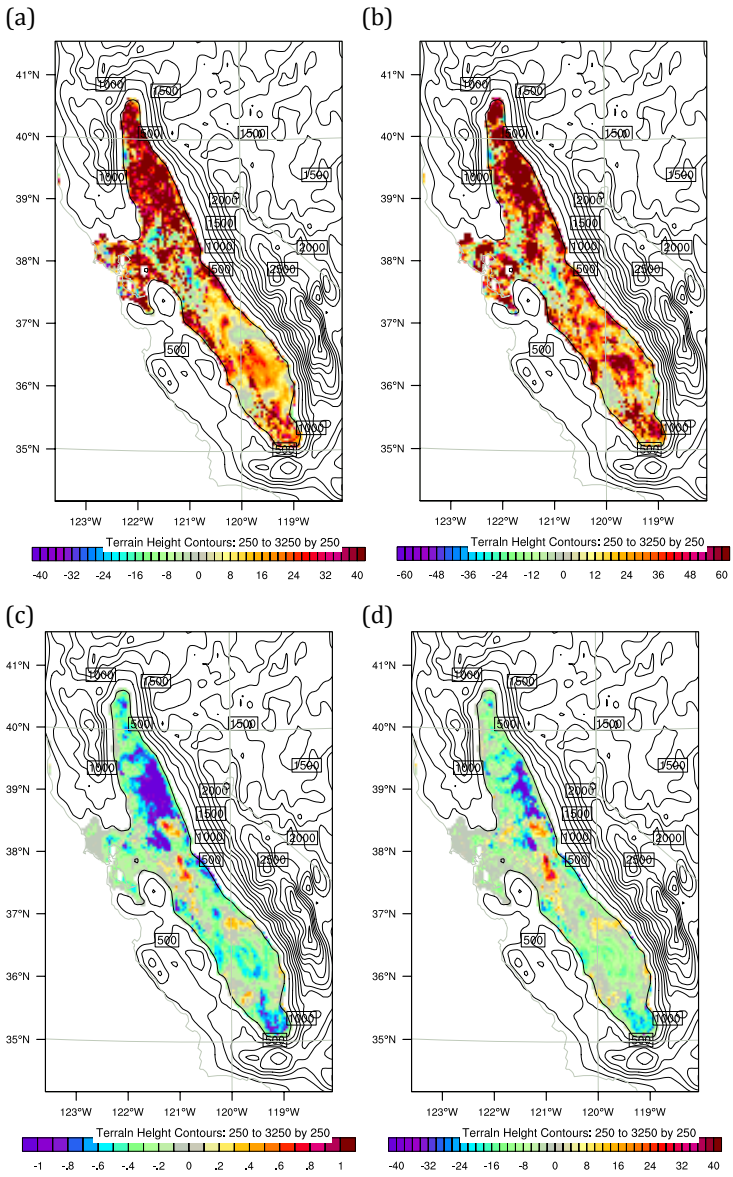

Figure 12. Relative change ((internally mixed – source-oriented)/source-oriented * 100%) in the daytime averaged predictions during 16 to 18 January 2011 for (a) the ratio of cloud water mixing ratio, (b) cloud droplet number and absolute difference (internally mixed – source-oriented) in (c) surface skin temperature (K) and (d) net shortwave radiation (W m^{-2}). (a) and (b) are average values using data within the first five model layers. Contours are terrain heights in m.

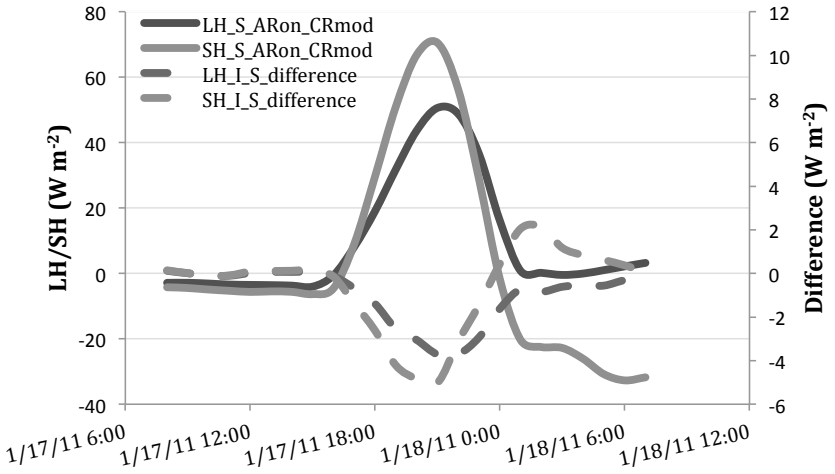

Figure 13. Area average of latent heat flux (LH) and sensible heat flux (SH) over the Central Valley in S_ARon_CRmod and the average difference between I_ARon_CRmod and S_ARon_CRmod from 0800 UTC 17 January (00 Z local time) to 0700 UTC 18 January (23 Z local time).